Chaos

High-frequency oscillations in the ripple bands and amplitude information coding: Toward a biomarker of maximum entropy in the preictal signals

Cite as: Chaos **32**, 093151 (2022); https://doi.org/10.1063/5.0101220
Submitted: 30 May 2022 • Accepted: 29 August 2022 • Published Online: 30 September 2022

Mauro Granado, Santiago Collavini, Roman Baravalle, et al.

High-frequency oscillations in the ripple bands and amplitude information coding: Toward a biomarker of maximum entropy in the preictal signals

Cite as: Chaos **32**, 093151 (2022); doi: 10.1063/5.0101220
Submitted: 30 May 2022 · Accepted: 29 August 2022 ·
Published Online: 30 September 2022

Mauro Granado,[1] Santiago Collavini,[2,3] Roman Baravalle,[1] Nataniel Martinez,[4] Marcelo A. Montemurro,[5] Osvaldo A. Rosso,[1,6] and Fernando Montani[1,a)]

AFFILIATIONS

[1]Instituto de Física de La Plata (IFLP), Universidad Nacional de La Plata, CONICET CCT-La Plata, Diagonal 113 entre 63 y 64, La Plata 1900, Buenos Aires, Argentina
[2]Instituto de Electrónica Industrial, Control y Procesamiento de Se nales (LEICI), Facultad de Ingeniería, Universidad Nacional de La Plata (UNLP-CONICET), La Plata 1900, Buenos Aires, Argentina
[3]Unidad Ejecutora de Estudios en Neurociencias y Sistemas Complejos (ENyS), Hospital El Cruce, Universidad Nacional Arturo Jauretche (HEC-UNAJ-CONICET), Florencio Varela 1888, Buenos Aires, Argentina
[4]Instituto de Física de Mar del Plata, Universidad Nacional de Mar del Plata & CONICET, Mar del Plata 7600, Buenos Aires, Argentina
[5]School of Mathematics & Statistics, Faculty of Science, Technology, Engineering & Mathematics, The Open University, Walton Hall, Milton Keynes MK7 6AA, United Kingdom
[6]Instituto de Física, Universidade Federal de Alagoas (UFAL), BR 104 Norte km 97, 57072-970 Maceió, Brazil

Note: This article is part of the Focus Issue on Complex Systems and Inter/Transdisciplinary Research.
[a)]**Author to whom correspondence should be addressed:** f.montani@fisica.unlp.edu.ar

ABSTRACT

Intracranial electroencephalography (iEEG) can directly record local field potentials (LFPs) from a large set of neurons in the vicinity of the electrode. To search for possible epileptic biomarkers and to determine the epileptogenic zone that gives rise to seizures, we investigated the dynamics of basal and preictal signals. For this purpose, we explored the dynamics of the recorded time series for different frequency bands considering high-frequency oscillations (HFO) up to 240 Hz. We apply a Hilbert transform to study the amplitude and phase of the signals. The dynamics of the different frequency bands in the time causal entropy-complexity plane, $H \times C$, is characterized by comparing the dynamical evolution of the basal and preictal time series. As the preictal states evolve closer to the time in which the epileptic seizure starts, the, $H \times C$, dynamics changes for the higher frequency bands. The complexity evolves to very low values and the entropy becomes nearer to its maximal value. These quasi-stable states converge to equiprobable states when the entropy is maximal, and the complexity is zero. We could, therefore, speculate that in this case, it corresponds to the minimization of Gibbs free energy. In this case, the maximum entropy is equivalent to the principle of minimum consumption of resources in the system. We can interpret this as the nature of the system evolving temporally in the preictal state in such a way that the consumption of resources by the system is minimal for the amplitude in frequencies between 220–230 and 230–240 Hz.

iEEG permits us to describe deep brain electrical activity. In this work, we investigate the dynamics of preictal and basal signals in patients with refractory epilepsy using entropy and complexity quantifiers. Our results show that minutes before the epileptic seizure, the system evolves from a highly dissipative chaotic state of the basal period to a state where the entropy reaches a maximum and the complexity is significantly curtailed, corresponding to the preictal period.

I. INTRODUCTION

An oscillatory system is characterized by positive feedback and the existence of restoring forces on it. Systems with restoring forces but without feedback can only maintain a transient oscillation with decreasing amplitude, a phenomenon called "resonance."[1] Neurons and neural networks with these properties preferentially evaluate inputs whose frequency matches frequencies that coincide with their own resonance. In particular, the neural oscillators belong to the family of limit cycle or weakly chaotic oscillators.[2] The oscillators underpinning brain dynamics can be characterized by two types: harmonic and relaxation oscillators, which tend to be exploited individually but also in combination.[1] Harmonic oscillators are good long-term predictors because their phase remains constant, whereas relaxation oscillators can be synchronized quickly and efficiently. Individual neurons oscillate mainly because voltage-dependent ion channels with opposite properties depolarize and hyperpolarize their membranes.[3] Due to the differential distribution of ion channels in soma-dendritic domains, neurons can have multiple oscillation and resonance properties. These properties can be dynamically adjusted either by changing the input resistance of the neuron or by affecting the probability with which a channel is open. For instance, interneurons are a class of neurons that are especially prone to resonate, which is why they are the basis for the construction of oscillatory mechanisms of a network.[4] Furthermore, the collective behavior of neurons is established through synchrony, which is denoted as the time in which some trace of a previous event generated by an input is retained, changing then the response to a subsequent event to other inputs.[5–11] Events that can be integrated over time by target neurons are of the synchronous type. The phenomenon of neuronal population synchronization improves the effective output of the neuron population, and this phenomenon can also arise without alternation of the firing rates of the neurons.[5–12] Thus, synchronization by oscillation is a metabolically economical mechanism to achieve a high impact in the network efficiency.[8–10] Specifically, we are interested in this specific kind of brain activity and the mechanisms that generate these phenomenon,[1,13–15] which can be identified as rhythmic electrical activity that takes place in the neural cortex spontaneously or as response to stimuli. How these oscillations are related to human perception, cognition, and behavior and how functional failures are related to neuronal deceases remain still unknown.

The activity of the human brain is extraordinarily complex;[1,16–19] we can safely say that the brain is the most complicated organ created by nature. Indeed, its complexity is due to the interaction of 100×10^9 nerve cells and much more contact points between them which provide our brain with capabilities that no supercomputer can match to this day. In 1926, Hans Berger performed the first ever EEG and discovered that brain activity was dominated by rhythmic signal fluctuations, a phenomenon known as brain oscillations.[1] Considering that from the time of discovery of brain oscillation to the current era, the recording and theoretical analysis techniques have been significantly improved, and it can be expected, therefore, significant breakthroughs in the area. In addition, intracranial electroencephalography (iEEG) is used to describe electrical activity in deep parts of the brain. The discovery of the iEEG signal containing useful information at frequencies higher than the traditional 100 Hz limit has had a profound impact on the understanding of brain function.[20] This type of oscillatory activity is commonly referred to as "high-frequency oscillations" (HFOs). Currently, HFOs are subclassified into ripples (80–250 Hz) and fast ripples (250–600 Hz).[21] Over the years, several studies supported by improved recording and analysis techniques have provided evidence that certain brain oscillations associated with HFOs were particularly important and useful in understanding epilepsy by describing the morphological, clonal, and pathophysiological signatures of epileptic events.[21] How brain oscillations may play a causal role in neurological disorders and what is its functional relevance is still a matter of current research.

The hypothetical mechanisms responsible for the generation of HFO are several. First, we can find the ephaptic interactions,[22] then electrotonic coupling through gap junctions,[23] and finally, the fast synaptic transmission.[24] At the cellular level, as epilepsy arises from uncontrollable neuronal excitation, it has been proposed that HFOs mainly reflect neuronal action potentials and could be generated by synchronized rapid firing of interconnected hyperexcitable neurons.[25] The discovery of this type of oscillations in epileptogenic activity was made in 2006 by Jirsch[26] who, based on deep electrode recordings in patients with focal epilepsy by spectral and visual analysis, was able to detect this type of behavior. This work allowed a breakthrough in the understanding of epilepsy, regarding the characterization of HFO prior, during, and after the epileptic crisis. Continuing with this line of research, subsequent studies were able to observe that during the preictal period exists an increase in HFO activity, although no systemic change in HFO could be observed.[27] On the other hand, further epilepsy studies have observed that different changes in the oscillatory activity of HFO during the preictal period could be detected only in the instants immediately prior to the ictal onset.[28] In this way, HFO on intraoperative electrocorticography (ioECoG) can be recorded over and around the possible lesion and can be used to delineate the epileptogenic tissue.[29] In particular, it has been demonstrated that in a significant percentage of patients with refractory epilepsy who underwent surgical intervention, the removal of brain tissue that generates HFO is associated with a better postoperative outcome compared with the removal of the zone identified with ictal onset (ZII).[30] Epilepsy surgery shows to be an effective treatment for drug-resistant focal epilepsy[31] where the resection of the HFO-rich area has been associated with good seizure-free outcome and the presence of postoperative ripples could predict seizure recurrence.[29,32,33] Nowadays, HFOs are promising interictal electroencephalographic biomarkers to identify the epileptogenic tissue[29,31,34,35] and may provide information about the region of the cortex that needs to be eliminated to achieve seizure control.[35]

Consistent with the results of research and clinical trials, HFOs are now being speculated as possible biomarkers for the identification of epileptic seizure due to the demonstrated increase in the spectral power of this high frequency band during the preictal period,[36] thus contributing to the information available for determining the epileptic seizure.[37] In the case of pathological HFO activity, each individual oscillation cycle appears to represent the ensemble firing of small groups of pathologically interconnected principal cells.[38] Morphological, molecular, and functional changes

in epileptic tissue cause neurons to respond abnormally to below-threshold stimuli or to become spontaneously active. In the current work, we investigate electrical recordings in patients with refractory epilepsy to discern the underlying oscillatory mechanisms during the epileptic process. To this end, the neuronal activity is studied for basal (far from the seizure) and preictal (immediately before the seizure) periods through recordings of intracerebral electrodes implanted in patients to achieve a greater resolution of local field potentials (LFPs). The intrinsic dynamics of the two types of recordings is discerned by using a time window analysis and studying the amplitude and phase for each signal through a Hilbert transform. The causality of these signals is quantified through information theory tools[15,39–41] and a symbolic method of analysis that accounts for the ordinal structure of them.[42–44] Importantly, our findings show that there is significant enhancing of Shannon entropy and the complexity is significantly curtailed in the range of HFO ripples within the preictal state in comparison to the basal signal. This allows us to find the potential biomarkers of the epileptogenic zone (EZ) characterizing the dynamics of different frequency oscillation bands.

II. RESULTS

A. Intracranial EEG

Epileptic seizure occurs when, due to a dysfunction in the brain,[45] a group of neurons begins to fire in an abnormal, excessive,[46] and synchronized way.[47] This results in a depolarization wave known as a "paroxysmal depolarization change."[48] For an epileptic seizure to occur, there must be a structural and/or functional change in the brain, with a reorganization of brain circuits. This phenomenon is called "epileptogenesis."

An epileptic seizure is a transient clinical event, which is characterized by the generation of electromagnetic discharges in the cerebral cortex. The neuronal electrical discharges of seizures are generated hypersynchronously and abnormally in the central nervous system.[49] These discharges occur suddenly, and their evolution is transient and short-lived, with a duration of about 2 min (this period is called "ictal"[49]). The temporal location of the recordings occurs approximately 40 min before the ictal onset.

The synchronized electrical activity of the neurons gives rise to LFPs and such activity can be measured through iEEG. There are physiological studies in which patients with epilepsy showed changes cardiovascular, metabolic, and in the LFP patterns a certain time before the epileptic seizure,[50] suggesting the possibility of seizure prediction. In this period, the rate of occurrence of spike activity patterns (involving focal and contralateral sites) increases significantly some time before the seizure originates.[51] In addition, other studies have detected a significant increase in the blood flow in areas involved in epilepsy that begins 10 min before seizure onset and 2 min before in lateral areas.[52,53] This characteristic time period prior to epileptic seizure generation is termed "preictal." The application of different methods has shown that abnormal activity in certain parts of the brain correlates bilaterally 20–30 min before the seizure.[54] In this work, we have considered a preictal period at about 10 min before seizure onset.

In recent years, advances in neurological knowledge and procedures have greatly improved the process of diagnosing epilepsy, where EEG continues to play a key role in the determination of the disease. In particular, interictal spikes are the most important marker for its diagnosis. While EEG is safe, painless, and noninvasive, its spatial limitation results in a restriction in the determination of EZ, which may lead to incomplete or mistaken removal during surgical treatment. Therefore, due to the restrictions of surface EEG or neuroimaging techniques, it is often necessary to perform an invasive procedure to record intracranial LFPs in order to more accurately record neuronal electrical activity. This procedure called iEEG has its main advantage of being able to directly record the LFPs coming from a set of neighboring neurons, with respect to traditional EEG. The experimental setup of the iEEG system is shown in Fig. 1, where we can observe "deep electrodes" implanted. These types of electrodes are made of a long and thin polyurethane rod with a diameter in the order of millimeters and have multiple contacts positioned equispaced all along them to record the LFP adjacent to them. This type of electrode is implanted inside the brain in order to record mainly the electrical activity of subcortical and cortical structures.

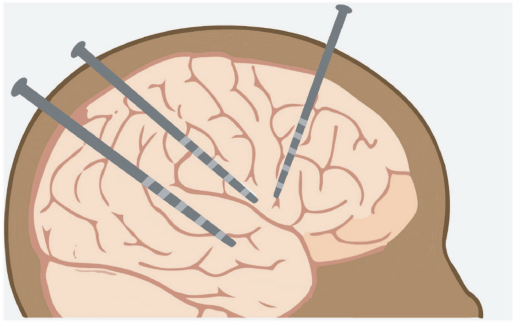

FIG. 1. Schematic drawing of a multi-electrodes array showing an implantation of them for iEEG recording.

Preictal states have been pointed out as a possible biomarker of focal epilepsy,[50] as evidence suggested that the onset of seizure may be preceded by a prognostic condition known as preictal state, which may help to predict seizure. These predictive states can be interpreted as deviations from the baseline signal. Figure 2 shows a typical raw signal for one of the channels of intracranial electrodes depicted in Fig. 1 (we refer the reader to Appendix B for further details of the data). Note that iEEG shows the activity of specific brain areas; however, the preictal signal does not in principle show visible deviations from the basal signal with the naked eye. A deeper analysis is, therefore, required to analyze possible differences between basal and preictal signals. This would require an appropriate theoretical framework to gain a better understanding of the possible different dynamics between baseline and preictal signals.

B. Quantifying the differences between different states

To split individual measures, the LFP is generally divided into distinct frequency bands, each of them characterized by a time-dependent amplitude and phase. This can be performed using a Hilbert transform that allows a proper extraction of the amplitude

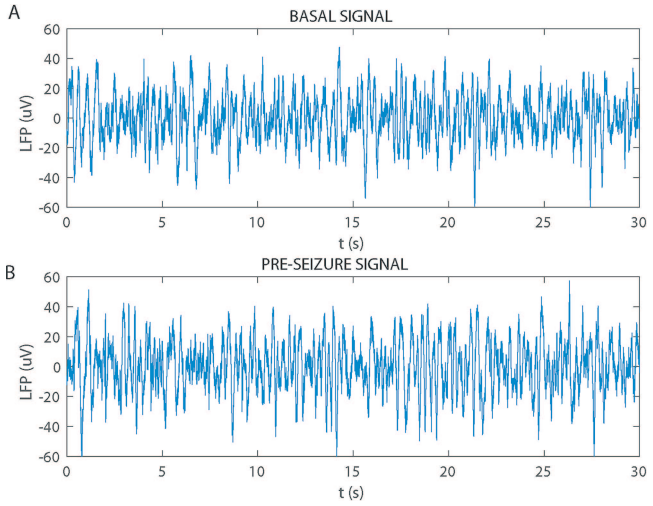

FIG. 2. Typical LFP recording made with deep electrodes in a subcortical area, where the voltage is displayed as a function of time. Note that (a) and (b) show the basal and preictal signals, respectively.

and phase of the LFPs signal to perform thereafter a more subtle processing. The Hilbert transform for a given signal $x(t)$ is defined as[7,55]

$$\hat{x}(t) = \check{H}(x(t)), \tag{1}$$

where

$$\check{H}(x(t)) = \frac{\int_{-\infty}^{\infty} \frac{x(t)}{t-\tau} d\tau}{\pi}, \tag{2}$$

which can be rewritten as

$$\check{H}(x(t)) = x(t) * \frac{1}{\pi t}, \tag{3}$$

where $*$ denotes the convolution operator.[55] The amplitude of the signal is defined as $a(t) = \sqrt{x^2 + \hat{x}^2}$, while the phase of the signal reads as $\phi = \arctan(\frac{\hat{x}}{x})$.

In the current analysis, we consider iEEG recordings from six patients with refractory epilepsy (three of them are presented in this section and the other three can be found in the subsec. 2c of Appendix A). The equipment used for the register had a sampling frequency of up to 2 KHz and allowed us to acquire the HFO ripples activity. To increase the resolution of the signal and to remove interference such as $1/f$ noise, this signal was filtered between 0.5 and 240 Hz using filtering based on "Kaiser windows," developed by Belitski.[56] The different frequency bands that we consider for analysis in the present work are composed of Berger bands and HFO bands up to 240 Hz (see Sec. 2 of Appendix B). The underlying idea is to study whether it is possible to determine, for different oscillation bands, possible biomarkers of refractory epilepsy by means of statistical complexity and entropy estimates of the amplitude and phase of the signal. For this purpose, we will use these quantifiers to investigate possible differences between basal and preictal signals (for further details of the information theoretical quantifiers being

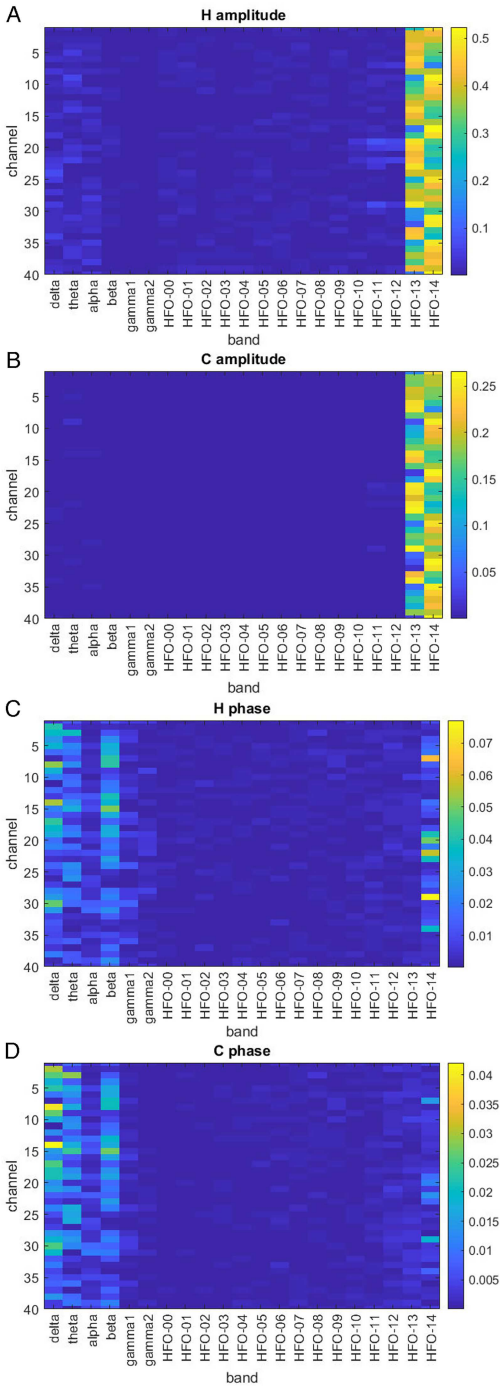

FIG. 3. Absolute value of subtraction for Shannon entropy and statistical complexity between the preictal and basal signals for the 40 channels and each frequency band, with respect to both amplitude and phase. The figure shows the results of a specific seizure event for the first subject. (a) Entropy, H, of the amplitude. (b) Complexity, C, of the amplitude. (c) Entropy, H, of the phase. (d) Complexity, C, of the phase. We used $D = 3$ and $\tau = 1$.

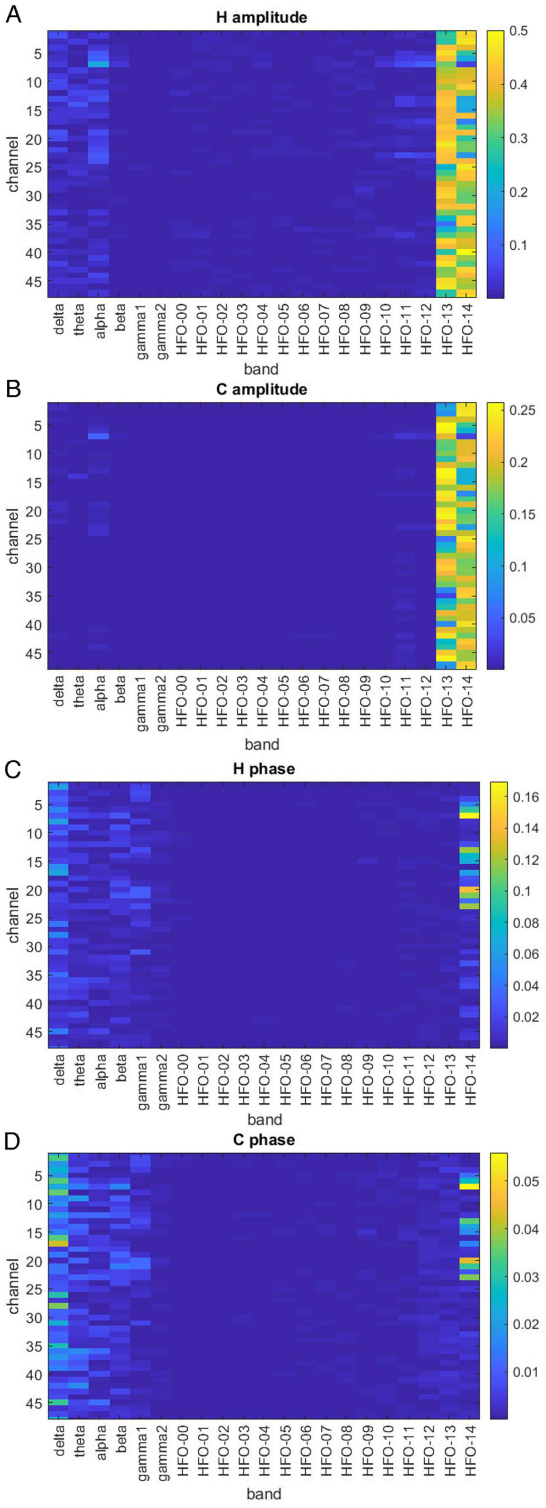

FIG. 4. Same as in Fig. 3 but for the second subject.

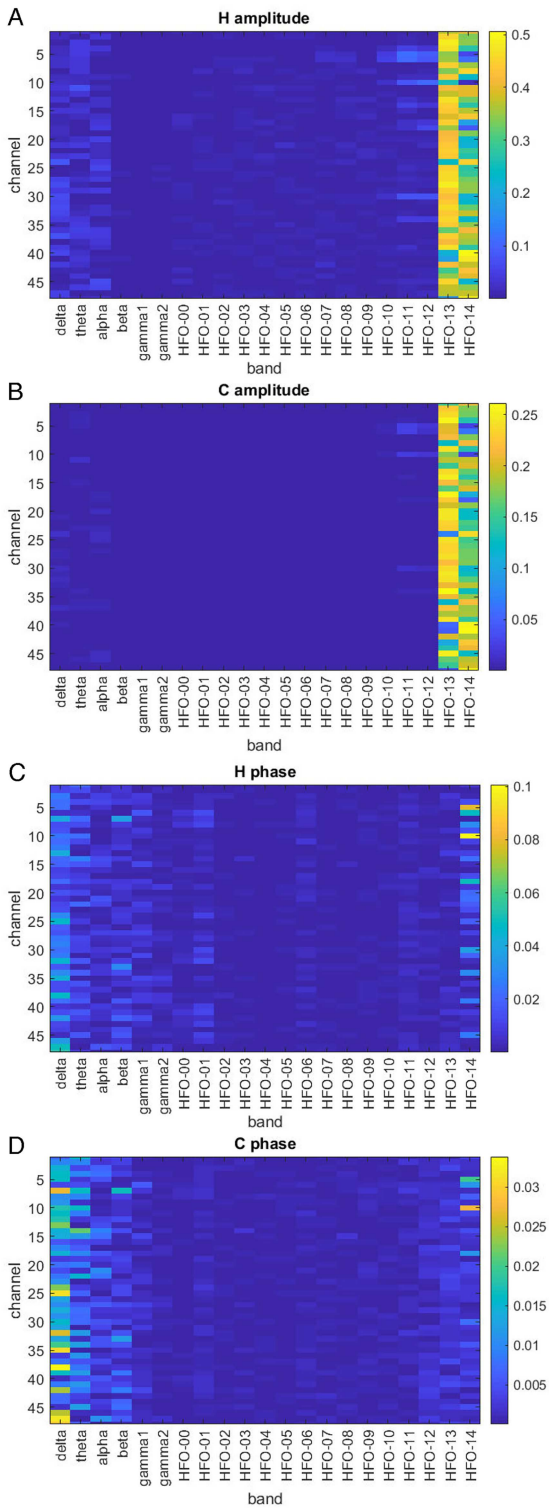

FIG. 5. Same as in Fig. 3 but for the third subject.

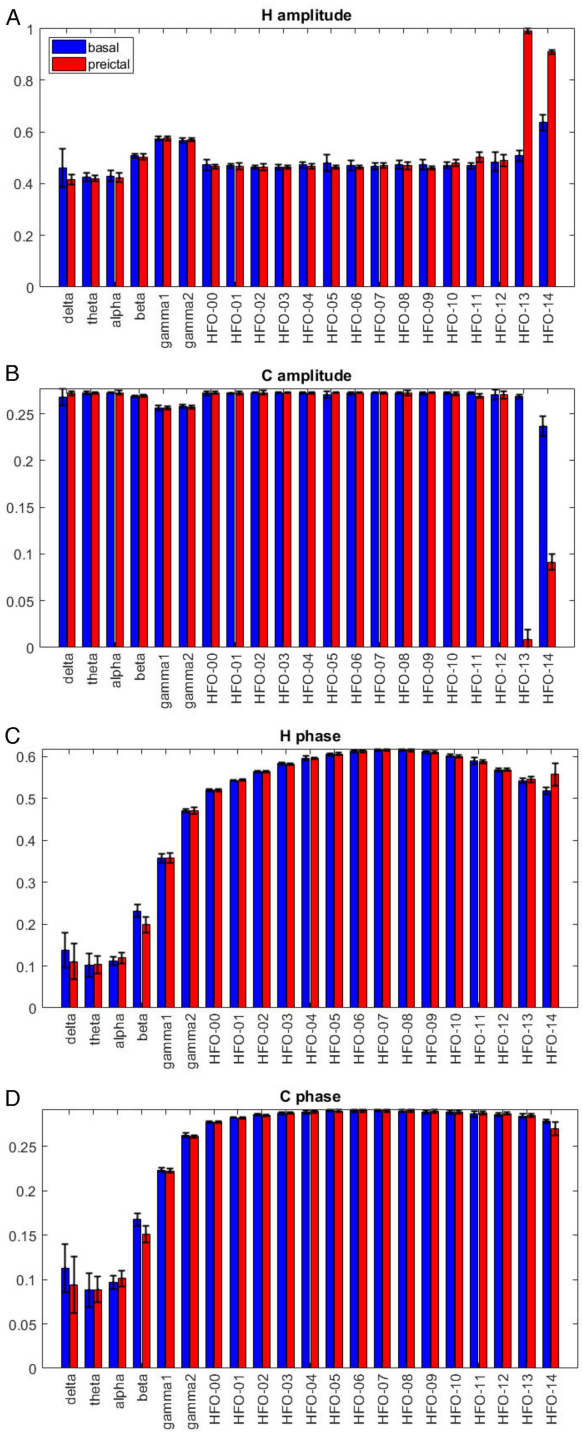

FIG. 6. Shannon entropy and statistical complexity for entropy and phase, for the channel number 23, considering basal and preictal signals of the first subject. (a) Entropy, H, of the amplitude. (b) Complexity, C, of the amplitude. (c) Entropy, H, of the phase. (d) Complexity, C, of the phase. We used $D = 3$ and $\tau = 1$.

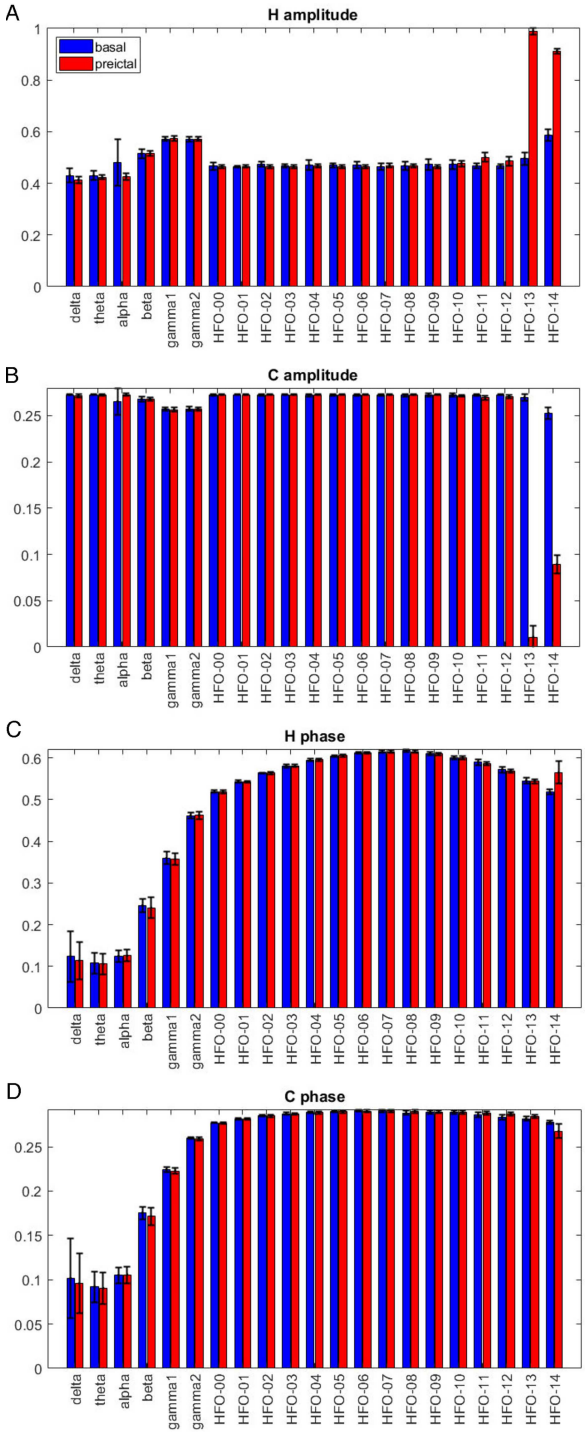

FIG. 7. Shannon entropy and statistical complexity for entropy and phase, for the channel number 41, considering basal and preictal signals of the second subject. (a) Entropy, H, of the amplitude. (b) Complexity, C, of the amplitude. (c) Entropy, H, of the phase. (d) Complexity, C, of the phase. We used $D = 3$ and $\tau = 1$.

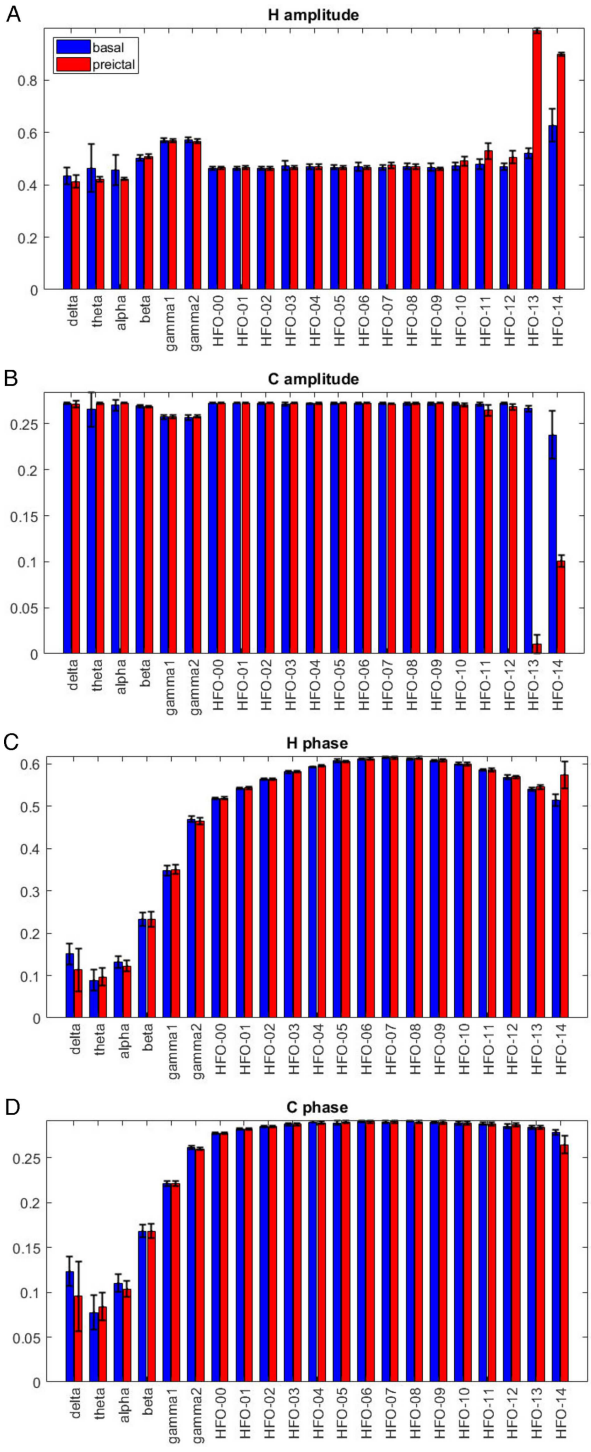

FIG. 8. Shannon entropy and statistical complexity for entropy and phase, for the channel number 4, considering basal and preictal signals of the third subject. (a) Entropy, H, of the amplitude. (b) Complexity, C, of the amplitude. (c) Entropy, H, of the phase. (d) Complexity, C, of the phase. We used $D = 3$ and $\tau = 1$.

used in this work, see Appendix A). Applying information theory tools, the spatiotemporal characteristics of the phase and amplitude of the basal/preictal signal were examined, for the electrical recording measured by electrodes implanted in different areas of the cortex, in terms of different frequency bands studied (from 0.5 to 240 Hz). With respect to the quantifiers of information theory, the Shannon entropy and the measure of statistical complexity were calculated for these signals through Bandt–Pompe methodology,[42] which builds a discrete probability distribution function (PDF) associated with the time series under study. The unique condition for the applicability of this methodology is that series should satisfy weak stationarity.[42–44]

Figures 3(a) and 3(c) show the absolute value of subtraction between the Shannon entropy of preictal and basal signals considering the amplitude and phase, respectively, for the total 40 channels of all intracranial electrodes implanted in the first patient for a specific seizure event that showed significant differences in both signals. Figures 3(b) and 3(d) are the same as in (a) and (c) but for the case of the statistical complexity. In both cases, the HFO-13 and 14 frequency bands show statistically significant differences performing a T-test for the Shannon entropy and complexity when considering the amplitude, while the phase shows a small variation for the theta, beta, and HFO14 bands. A similar behavior for subtraction between the Shannon entropy of preictal and basal states, for the second and third patient, can be observed in Figs. 4(a), 4(c), Figs. 5(a), and 5(c), respectively. In both patients, the number of total channels from all the intracranial electrodes implanted is 45. Moreover, Figs. 4(b), 4(d), 5(b), and 5(d) exhibit similar behavior for subtraction between the complexity of preictal and basal states in the case of second and third patients, respectively. For second and third subjects, we have also considered a specific seizure event that showed significant differences in both signals.

In the following we show results for Shannon entropy and statistical complexity for three of the six subjects under study, but now just taking into account a particular channel of the seizure event considered above that showed the most significant statistical differences individually in each of the three subjects. Figure 6 shows the results of Shannon entropy and statistical complexity for amplitude and phase, for the channel number 23, considering basal and preictal signals of the first subject (and the same seizure event as the one selected above). Through bar charts, we compare groups of data that correspond to the basal and preictal signal for the information quantifiers. Note that in Fig. 6(a) for the case of the amplitude in the frequency bands HF0-13 and 14, the Shannon entropy is significantly higher for preictal states compared to the basal ones. In contrast Fig. 6(b) shows the opposite behavior, that is the complexity being significantly higher in the basal state in comparison to the preictal state for HF0-13 and 14. For the rest of the bands, no significant differences are observed in the amplitude, although there is a slight effect in the theta band where the Shannon Entropy is higher in the basal signal than the one of the preictal state. Let us note in Figs. 6(c) and 6(d) that for phase, the Shannon entropy and statistical complexity are higher for the basal state than the preictal state, when considering the beta band. Moreover, the Shannon entropy of the phase is significantly higher in the preictal state, for the HFO-14 frequency band, in comparison to the basal signal. There is also a slight effect in the theta band; however, it is not statistically significant.

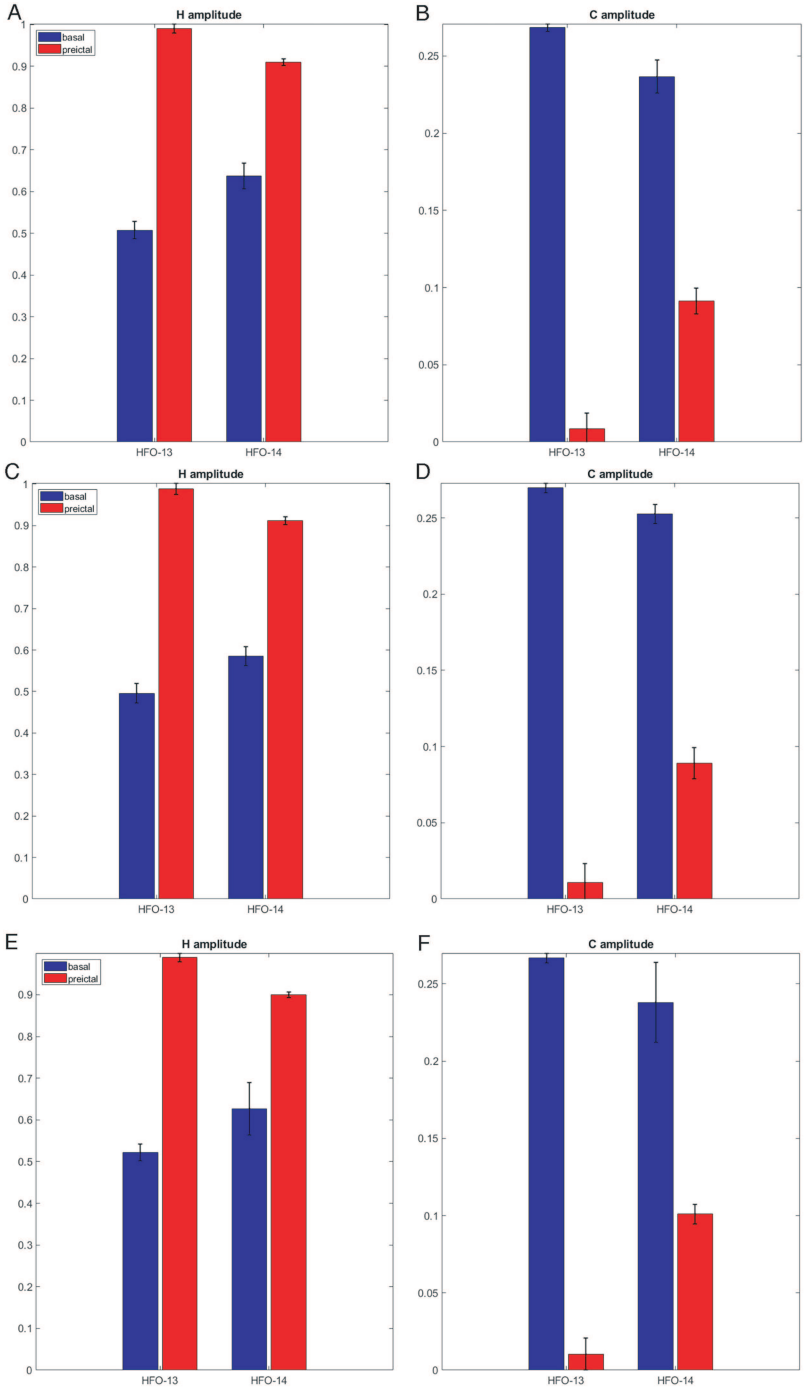

FIG. 9. Basal and preictal signals for HFO 13 and 14. (a) Entropy, H, and (b) complexity, C, of the amplitude for the first subject. (c) Entropy, H, and (d) complexity, C, of the amplitude for the second subject. (e) Entropy, H, and (f) complexity, C, of the amplitude for the third subject. We used $D = 3$ and $\tau = 1$.

Figures 7(a) and 7(b) depict the Shannon entropy and statistical complexity of the amplitude for the second patient, with the seizure event selected above for this subject, considering the channel 41. Figures 7(c) and 7(d) depict the Shannon Entropy and the Statistical complexity of the phase for the second patient taking into account the same seizure event. Figures 8(a)–8(d) are the same as above but for the third patient, with the same seizure event selected above for this subject and for channel 4. We can particularly observe in these cases that there are very significant differences, for both information quantifiers, between basal and preictal states of the amplitude when

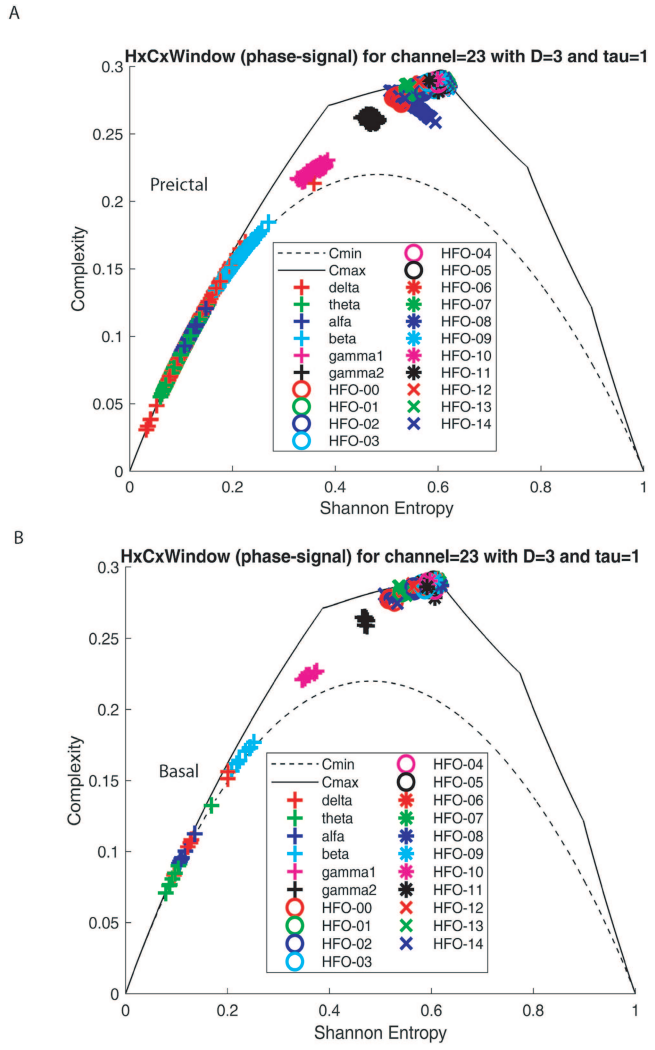

FIG. 10. $H \times C$-plane of the phase, first subject, taking into account different frequency bands. We consider $D = 3$ and $\tau = 1$. (a) Preictal state; (b) basal state.

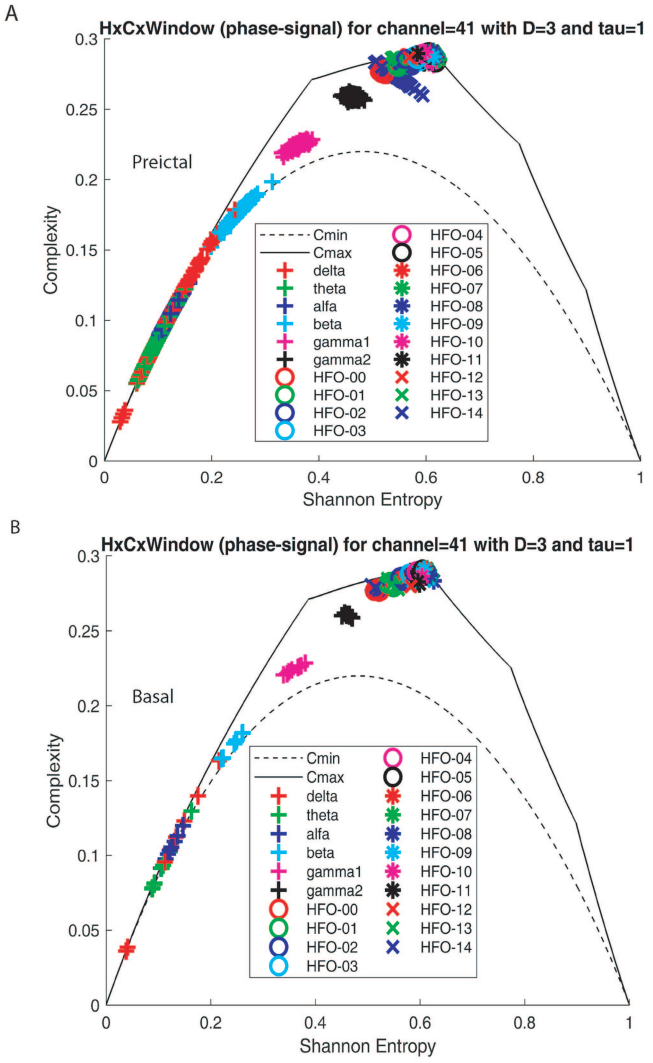

FIG. 11. $H \times C$-plane of the phase, second subject, taking into account different frequency bands. We consider $D = 3$ and $\tau = 1$. (a) Preictal state; (b) basal state.

taking into account HFO-13 and 14. That is, for second and third patients, the entropy corresponding to the amplitude is also much higher for HFO-13 and 14 frequency bands in the basal signal than for the preictal ones. On the other hand, the behavior of the complexity for the amplitude is such that it is much lower for the preictal signal than for the basal signal in HFO-13 and 14 frequency bands. We can also observe for both subjects that the Shannon entropy of the phase is also higher in the preictal state than the basal one for the HFO-14 band. We can see from previous figures that entropy and complexity of the amplitude remain approximately constant for all bands with the exception of HFO 13 and 14. In contrast, the entropy and complexity of the phase increase to a maximum at HFO 7 and 8 and then slightly decrease its value. Significant differences in entropy and complexity values for the phase between basal and preictal states for the three subjects shown in this section can be appreciated in the HFO-14 frequency band. The entropy and complexity estimations were made for a time series of 10 min taking time windows of 4 s, which allowed us to have 2000 points for each of them, ensuring a much smaller embedding dimension ($D = 3$ in all cases, $D = 4$ and 5 do not significantly change the results) than the size of the time series. The values shown correspond to the averages of these time windows that ensure their robustness. Overall, our findings show that the ripple bands corresponding to HFO-13 and HFO-14 depict very significant differences, between basal an preictal states, for both information quantifiers in the case of the amplitude. This can be further appreciated in Figs. 9(a), 9(c), and 9(e) that depict the basal

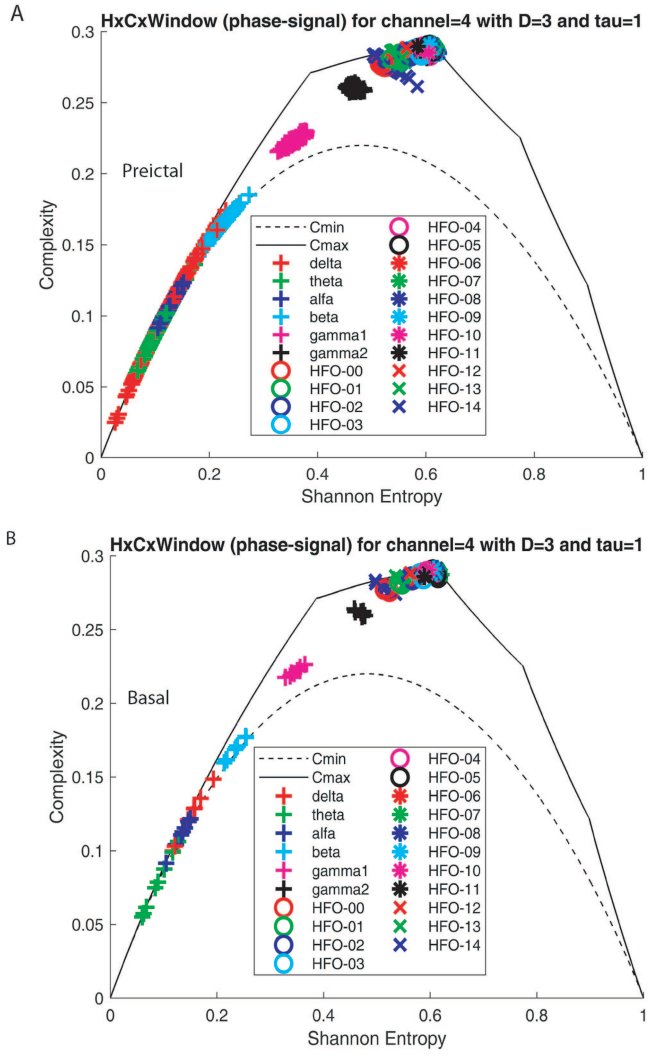

FIG. 12. $H \times C$-plane of the phase, third subject, taking into account different frequency bands. We consider $D = 3$ and $\tau = 1$. (a) Preictal state; (b) basal state.

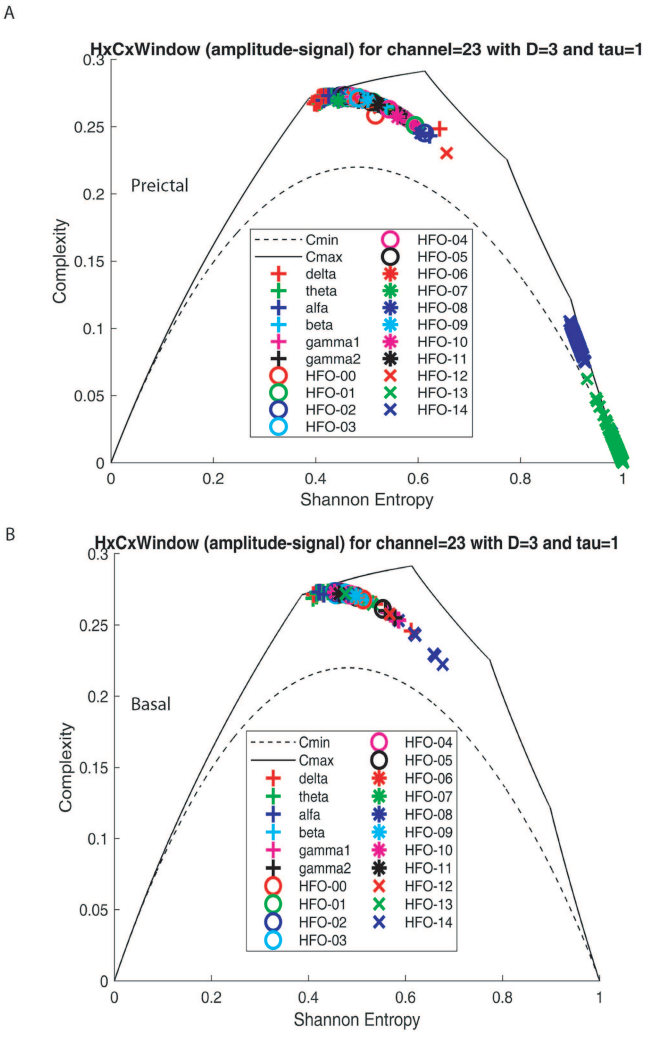

FIG. 13. $H \times C$-plane of the amplitude, first subject, taking into account different frequency bands. We consider $D = 3$ and $\tau = 1$. (a) Preictal state; (b) basal state.

and preictal Shannon entropy for the amplitude of the signal for first, second, and third subjects, respectively. Notice from Figs. 9(a), 9(c), and 9(e) that Shannon entropy is significantly increased for HFO13-14, in the case of preictal signals in comparison to the basal ones, for three subjects under consideration. In contrast Figs. 9(b), 9(d), and 9(f) show that the complexity is significantly curtailed for the HFO13-14, in the case of preictal signals in comparison to the basal ones, in all cases being analyzed.

C. Analysis of temporal dynamics considering the entropy complexity plane

The $H \times C$ plane is based only on global features associated with the time series under study.[15,39–41] Investigating the plane $H \times C$ provides information related to the correlated structure between the components of the system. Since the complexity is defined in terms of the normalized Shannon entropy H [Eq. (A8), see Sec. 2a of Appendix A], it can be seen that, for a given value of this magnitude, the range of possible values of C are determined between a $C_{\min}$ and a $C_{\max}$ curve, which depend only on the number of degrees of freedom (D) considered for the Bandt and Pompe probability function. This is due to the fact that the calculation of the complexity depends on two different PDFs, one corresponding to the system under study P and the other to the equilibrium distribution P_e, thus restricting the possible values of the statistical complexity in the $H \times C$ plane.[57] This type of methodology allows to investigate the non-stationary behavior of a time series associated with neuronal activity measured in the LFPs,[15] to discover important details concerning the ordinal

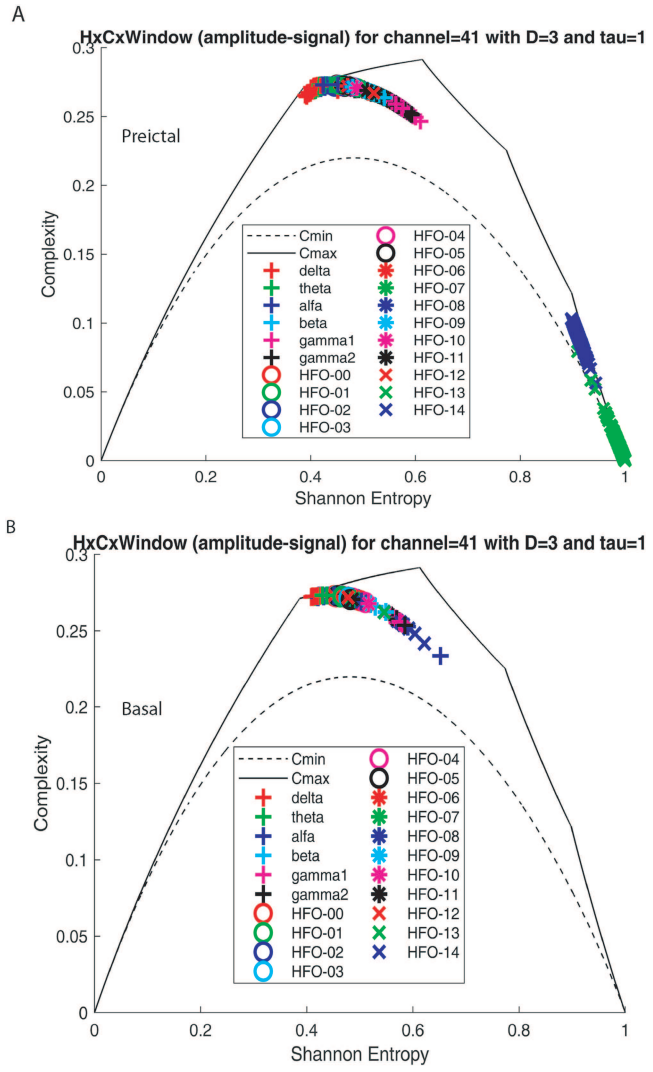

FIG. 14. $H \times C$-plane of the amplitude, second subject, taking into account different frequency bands. We consider $D = 3$ and $\tau = 1$. (a) Preictal state; (b) basal state.

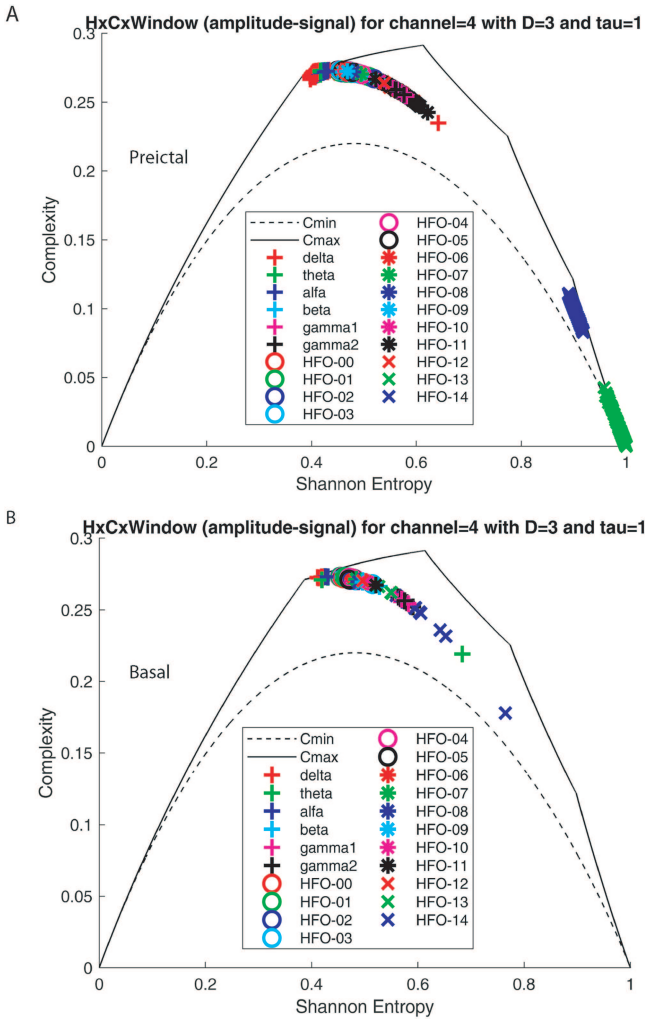

FIG. 15. $H \times C$-plane of the amplitude, third subject, taking into account different frequency bands. We consider $D = 3$ and $\tau = 1$. (a) Preictal state; (b) basal state.

structure of the time series,[58–61] and also to obtain information about temporal correlations.[62]

The complexity planes $H \times C$ were constructed from the corresponding information theory quantifier. The assessment of the $H \times C$ plane for the phase of the preictal signal can be seen in Figs. 10(a), 11(a), and 12(a) for first, second, and third patients, respectively. The $H \times C$ plane of the phase for basal signals is shown in Figs. 10(b), 11(b), and 12(b) for first, second, and third patients, respectively. Let us notice that there are interesting differences in the temporal evolution of the LFP time series, for the different time windows, between preictal and basal states for theta, beta, and HF014 bands.

The estimation of the $H \times C$ plane for the amplitude of the preictal signal can be seen in Figs. 13(a), 14(a), and 15(a) for first, second, and third patients, respectively. In contrast, the $H \times C$ plane of amplitude of basal signals is shown in Figs. 13(b), 14(b), and 15(b). We have considered as in the figures of Sec. II B, for each subject, the channels of interest belonging to seizure events that showed significant differences in information quantifiers between basal and preictal activities for the three subjects under study with refractory epilepsy (results for another three subject are presented in the Sec. 2c of Appendix A). Entropy can be considered as a measure of how close or not a system is to equilibrium; it can also be considered as a measure of the disorder (spatial and thermal) of the system. The second law of thermodynamics states that the entropy, or disorder, of an isolated system can never decrease. Therefore, when

an isolated system reaches a configuration of maximum entropy, it can no longer undergo changes: it has reached equilibrium. In such cases, the system seems to "prefer" disorder, and in the case of refractory epilepsy, the amplitude of the preictal signal for HFO 13-14 frequency bands behave "as if it were an isolated system" that has reached equilibrium. The $H \times C$ planes show that as the system evolves, becoming closer and closer to the end of the preictal state and the beginning of the seizure, the complexity of the amplitude of the preictal signal becomes more and more curtailed and tends to zero, while in contrast the entropy is approaching one and, therefore, reaches its maximum value. This can be seen in Figs. 13(a), 14(a), and 15(a) where the direction of the temporal evolution of different time windows is in the "orientation" in which entropy grows and the complexity is curtailed. In Sec. 2c of Appendix A, we show that the results for the $H \times C$ planes of fourth, fifth, and sixth patients have a similar behavior to the one presented in the figures above. Thus, as entropy increases and complexity decreases, for the amplitude in the preictal signal, the system gets more and more closer to the ictal state where the epileptic seizure will show the anomalous hypersynchronous discharge. Thus, one could conclude that the system reaches a thermal state of equilibrium in HFO13 and 14 frequency bands, in which all states tend to be equiprobable with very low complexity, preceding the epileptic seizure.

D. Discussion and conclusions

For an epileptic seizure to occur, there needs to be a structural and/or functional change in the brain, with a reorganization of brain circuits. This particular phenomenon called "epileptogenesis" is responsible for facilitating synchronization and discharges of large neuronal populations during seizures. Thus, epileptogenesis is understood as the process by which a particular neuronal group or circuit becomes hyperexcitable and can spontaneously generate epileptic seizures.[63] This mechanism can be observed in patients with epilepsy resulting from a lesion in the brain, where the injured area results in up-regulation of excitatory circuits and down-regulation of inhibitory circuits.[64]

The EZ is a theoretical formulation that was initially defined as the site in the cerebral cortex where epileptic seizures are initiated and where the whole epileptic activity is primarily organised. In order to completely cease seizures, it is necessary and sufficient to remove (or disconnect) the area of the cortex corresponding to the EZ.[65] In the last decade, it was found that the EZ corresponded not only to a single brain area but to a neural network itself.[66] This network consists of an arrangement of cortical and subcortical brain structures that are anatomically and functionally connected, where electrical activity in any part of it affects the activity in the rest of it. The possibility of determining the location and organization of the neural network involved in the origin of the epileptic discharge is essential for the definition of the EZ.[67] In the present work, the electrode channels that showed significant differences between basal and preictal signals for Shannon entropy and complexity, which were shown in the Results section, were located in the left hippocampal body and head and in the left amygdala. This prediction coincides with determinations made by the neurologists team. Thus, the current methodology that characterize the differences between dynamics of the basal and preictal time series, through information-theory quantifiers, is a powerful tool for early detection of biomarkers of refractory epilepsy.

In the human brain, physiological high-frequency ripples (around 200 Hz) are mainly located in the CA1 region of the hippocampus and in the entorhinal cortex, where they are part of highly complex sharp-wave oscillation,[68] although they have also been found elsewhere. In particular, mesiotemporal HFOs are involved in memory formation and evocation of past experiences. As for the low-amplitude physiological HFO activity in the extratemporal neocortex, it seems to be related to information processing functions, just as it has been found in the extratemporal neocortex, in the same way as during somatosensory-evoked potentials.[69] HFOs are generated locally, and the synchronization mechanisms that induce these oscillations must be fast enough to be able to synchronize all the electrical activity of the entire spatial area under examination within 2–5 ms. In such area, the activation of a small neuronal population (or an individual neuron) can result in a fast recruitment of interconnected cells, resulting in a synchronous activation of the action potential, which is ultimately sensed in extracellular recordings as an HFO. In addition, the region in which HFO synchronization mainly occurs is spatially continuous, although sometimes this phenomenon can be in contacts separated by large distances.[70] Regarding the hypothetical mechanisms that are responsible for the generation of HFO, we can find first of all ephaptic interactions,[22] the electrotonic coupling across junctions[23] and finally fast synaptic transmission.[24] Therefore, each of the billions of neurons in our brain are elements of communication, where communication involves information.

The average "surprise" value of a variable is defined by its probability distribution and is called entropy. In particular, entropy is a measure of uncertainty. When we reduce our uncertainty, we gain information, so information and entropy are two sides of the same coin. The average amount of information shares somehow the same definition as entropy. If a variable has high entropy, the initial uncertainty about its value is large and, by definition, such systems are characterized by randomness. If we consider the average value of that variable, we have an amount of information that equals the uncertainty (entropy) we had about its value. Consequently, receiving an amount of information is equivalent to having lost exactly the same amount of entropy. Neural coding capacity is defined by the upper limit on entropy and, therefore, the amount of information transmissible by a neuron. This means that it is impossible to use a rate of activation of the dendritic spines that transmit more information than the coding capacity. In simple terms, entropy tells us how difficult it is to make predictions about events described by a probability distribution. The higher the entropy, the harder it is to make predictions. In addition, the maximum entropy principle states that the probability distribution that best represents the current state of knowledge about an isolated system is the one with the highest entropy, in the context of precisely expressed prior data (such as a proposition expressing testable information). That is, under this principle, we know exactly the prior data or we have verifiable information about a probability distribution function. Considering the set of all test probability distributions that would encode the prior data, according to this principle, the distribution with maximum

information entropy is the best choice for the system. That is, entropy in an isolated system never decreases because coupled systems evolve toward thermodynamic equilibrium that is given by the principle of maximum entropy. Our results show that as the preictal condition develops closer to the ictal state, for signal amplitudes of HFO bands between 220–230 and 230–240 Hz, the $H \times C$ dynamics draw nearer to maximum entropy and zero complexity. That is to say, the quasi-stable states converge to equiprobable states when the entropy is maximal, and the complexity is zero. We could, therefore, speculate that in this case it corresponds to the minimization of Gibbs free energy. We can say that for these ripple bands the system behaves as an"isolated system" that seeks to reach its equilibrium distribution with maximum entropy. The consumption of resources by the system is minimal, providing that the entropy of the system is "above some threshold." Thus, the principle of maximum entropy is equivalent to the principle of minimum consumption due to limiting resources by the system. This is somehow equivalent to the model of an ideal gas in which the equilibrium state minimizes the Gibbs free energy. Although scale-free dynamics generate complexity, neural oscillations exhibit high-order temporal correlations that are reflected in high complexity values within the basal signals for all the frequency bands.

The transient order of brain activity, in terms of system complexity, does not emerge from disorder but from an intermediate state between order and disorder. When necessary, neural networks are able to rapidly shift from a highly complex state with intermediate entropy for the basal signal to a system reaching maximum entropy and where the complexity is significantly curtailed due to the random nature in the amplitude of HFO13 and 14 in preictal states. We show using the planes $H \times C$ that the dynamics in the cerebral cortex for the amplitude of the basal signal is in a highly chaotic dissipative zone, with high complexity and intermediate entropy values. However, for the preictal state, the consumption of resources by the system is minimal for the amplitude in frequency bands between 220–230 and 230–240 Hz, as the system is highly random, and the complexity is significantly curtailed. In this case, the maximum entropy is analogous to the principle of minimum system resource consumption, which would be equivalent to Gibbs minimum free energy, because randomness and low complexity seem to be a condition for the preictal system amplitude in the case of frequency bands between 220–230 and 230–240 Hz. Also, all neurophysiological processes require energy and particularly brain energy consumption varies. When in "normal mode" or in basal state, consumption is lower than during the ictal condition, in the sense that no specific area of the brain is more activated than others. But, when the brain suddenly begins to process a preictal state, it prepares for an electrical storm that occurs due to the brain's hypersynchrony state in which the energy consumption will be enormous. Thus, the HFO frequency bands 13-14 appear in the preictal state using minimal system resources to adapt for an event that will trigger high energy expending during the epileptic seizure. Overall, we can conclude, therefore, that the complexity planes $H \times C$ constitute an excellent biomarker that anticipates spatially and temporally the areas where the epileptic focus is triggered. The current methodology could serve, therefore, as the basis for successful fast online software that would help neurologist to find seizure precursors in cases of refractory epilepsy.

ACKNOWLEDGMENTS

We are grateful for the collaboration of the Unidad Ejecutora de Estudios en Neurociencias y Sistemas Complejos (ENyS) for the electrophysiological recordings provided for the study carried out in this work. We thank funding from PUE 22920170100066CO IFLP-CONICET Argentina and Project No. 80120190100127LP Universidad Nacional de La Plata, Argentina. Also, we gratefully acknowledge Professor Araceli Billodas for helpful suggestions.

AUTHOR DECLARATIONS

Conflict of Interest

The authors have no conflicts to disclose.

Author Contributions

Mauro Granado: Conceptualization (equal); Data curation (equal); Formal analysis (equal); Investigation (equal); Methodology (equal); Resources (equal); Software (equal); Validation (equal); Visualization (equal); Writing – original draft (equal); Writing – review & editing (equal). **Santiago Collavini:** Data curation (equal); Software (equal); Validation (equal); Visualization (equal). **Roman Baravalle:** Investigation (equal); Methodology (equal); Software (equal); Visualization (equal). **Nataniel Martinez:** Software (equal); Validation (equal). **Marcelo A. Montemurro:** Methodology (equal); Software (equal); Visualization (equal). **Osvaldo A. Rosso:** Project administration (equal); Software (equal); Supervision (equal); Validation (equal). **Fernando Montani:** Conceptualization (equal); Data curation (equal); Formal analysis (equal); Funding acquisition (equal); Investigation (equal); Methodology (equal); Project administration (equal); Resources (equal); Software (equal); Supervision (equal); Validation (equal); Visualization (equal); Writing – original draft (equal); Writing – review & editing (equal).

DATA AVAILABILITY

The data that support the findings of this study are available from the corresponding author upon reasonable request.

APPENDIX A: THEORETICAL METHODS

A signal is usually defined as a convey of information about a phenomenon, so any given measure that could change over time or space can be considered as a signal. Based on their statistical properties, a signal can be considered as non-stationary or stationary. The main difference between stationary and non-stationary signals is that stationary process signals do not change in time, whereas non-stationary process signals change inconsistently along time. The activity reflected in neural signals is often non-stationary and has a broad frequency spectrum. The measurement of different non-stationary temporal sequences corresponding to observable constitutes the most important element of the experimental investigation of the dynamics of neural systems, i.e., the study of the temporal evolution of these phenomena. These sequences of data or measured values at a given time and chronologically ordered are known as "time series." That is, a time series is a succession of values indexed according to a t parameter, which are taken temporally

equidistant. These series are commonly used to study the causal relationship between different variables that evolve over time and influence each other. Information about the dynamics of the system under study can be extracted from the time series by means of various analytical methods.[71] If the elements of the time series form a family of random variables, it becomes a stochastic process, which is a mathematical model of a process that evolves randomly over time.[72] Each of the random variables in a stochastic process has its own probability distribution function and may or may not be correlated to each other. The "probability density function" (PDF) describes the relative probability of taking a certain value for a continuous random variable.[73] The probability that the variable randomly falls in a specific region of the probabilistic space will be given by the integral of the density of this variable between one and another limit of this region. The PDF satisfies being positive throughout its domain and its integral over all the space corresponds to the unit value. In the practical case, as in the present work, the time series tend to take discrete values given by instrumental limitations, the discretization of the evaluated data or by the digitization of data, among others. By having a discrete time series of random variables, we can express this as $\chi(t) = \{s_t; t = 1, \ldots, N\}$, with N being the total number of values that this series takes. When studying a discrete time series, the description of the probability about the possible states of it is given by the "probability function" (PF)[73] and in most cases is not trivial to calculate it. This function P associates probability p to each point in sample space, which is the set of all possible outcomes of a random experiment. In the continuous limit, the PF tends to be the PDF.

1. Bandt and Pompe methodology

To find the PDF corresponding to a given time series under analysis, the usual techniques assign a specific symbol to each recurrent value in this time series, thus constructing a symbolic sequence of the non-causal coarse-grained type that describes it. In this way, this type of methodology does not take into account the dynamics of the temporal scales or the ordering relationships that exist in the time series since a symbol is assigned to each element, resulting in the PDF having no temporal information whatsoever. An example of this type of methodologies are those based on the construction of histograms. As information about the temporal dynamics of the system is required in the symbolic sequence, the causal information must be duly incorporated by assigning these symbols to a portion of phase space or to a trajectory.

In 2002, Bandt and Pompe[42] proposed a very simple and robust method for analyzing time series, which does take into account the temporal structure of the time series generated by the process (i.e., it is a coarse-grained causal method). The causality of the "Bandt and Pompe methodology" (BPM) is mainly given by the comparison that is made between the nearest elements of the time series. Thus, opposite to most of techniques that are put into practice, the BPM considers the ordinal structures of the time series instead of just the time series values. Because of this, it allows us to discover important details regarding the ordinal structure of the time series[58–61] and also obtain information about the temporal correlations.[62,74]

The way in which this methodology evaluates the PDF associated to a scalar time series is based on a symbolization technique that basically consists of assigning to the series itself different symbolic sequences associated with the counting of ordinal patterns. As a result, the relevant symbolic data are made up from the classification of the elements of a given time series and also from the rearrangement of these integrated data in ascending order. Is because this ordering of the elements of the time series that the causal temporal information is obtained from the BPM.

It is worth noting that the appropriate sequence of symbolization arises naturally from the time series itself, making unnecessary to carry out any additional procedure. In fact, the partitions emerge automatically by comparing the neighborhood order of relative values rather than by assigning amplitudes according to different recorded levels as is done by conventional rank-based methods that partition the data (such as, PDFs constructed from histograms). This is why BPM is considered to be one of the simplest symbolic techniques that also incorporates temporal causality, and there are many studies describing the advantages that make the BPM as one of the most convenient[74–77]

On the other hand, it is clear that this type of analysis leads to the loss of the detail of time series amplitude information. In spite of this, by referring to the intrinsic structure of the series by means of the application of the BPM, only a significant reduction is achieved with respect to the characterization difficulty of the series. Furthermore, the cost-effectiveness of this methodology is optimal for the analysis of very long time series.

Another detail that makes the BPM excellent for the analysis of experimental data is that the ordinal patterns associated with the PDF are invariant with respect to non-linear monotonic transformations of associated distribution. That is, non-linear shifts or changes in scale introduced by the measuring device do not modify the estimation of the quantifiers, which is a significant property when working with experimental data. This implies that artificial scaling or non-linear changes introduced by the measuring instrument do not modify the calculation of the information quantifier estimated by this methodology.[78]

a. Ordinal patterns

The ordinal pattern of an n-tuple (a sequence of n elements) of real numbers $(x_0, x_1, \ldots, x_{n-1})$ describes how the elements of this relate to each other in terms of their positions and values. To establish an ordinal pattern, each element x_i of the n-tuple is designated with a "symbol" or index $r_i = \in \{0, 1, \ldots, n-1\}$, where the largest element of this will be assigned the index $n-1$, the second largest will be assigned the index $n-2$, and so on until the smallest of all, which will be assigned the $r_i = 0$. For example, the ordinal pattern corresponding to the 3-tuple $(15, 10, 13)$ will be $(r_0, r_1, r_2) = (2, 0, 1)$, which for the sake of simplicity we will denote as [201].

It is evident that only n-tuples of distinct elements can have an unambiguous ordinal pattern. To avoid ambiguity in the face of repeated values, one can consider that when two elements are equal, one is taken to be greater than the other in an arbitrary way. This arbitrariness can also be justified if the elements x_i belong to a continuous distribution, the probability that two values can be identical is zero.

Given an n-tuple, each permutation in the array of elements x_i results in a different ordinal pattern. Therefore, there exists an array

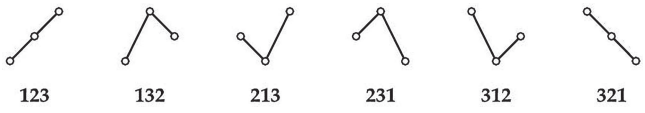

FIG. 16. Schematic representation of six possible ordinal patterns for the order $n = 3$.[79]

of $n!$ ordinal patterns,

$$\Omega = \{\Pi_1, \Pi_2, \ldots, \Pi_{n!}\}, \tag{A1}$$

for a given n-tuple. This is why we call n the order of the ordinal pattern (with $n \geq 2$).

Consider again as an example a generic 3-tuple (x_0, x_1, x_2) with $x_0 \neq x_1 \neq x_2$. For order $n = 3$, the $n! = 3! = 6$ possible ordinal patterns are denoted as

$$\Omega_3 = \{012, 021, 102, 120, 201, 210\}. \tag{A2}$$

In Fig. 16, we can observe the different diagrams of the six ordinal patterns corresponding to Ω_3. It can then be observed that any given sequence $(x_0, x_1, \ldots, x_{n-1})$ under the conditions mentioned above can be be mapped into a sequence of ordinal patterns in space Ω_n.

b. Constructing the ordinal pattern of a time series

Given a scalar and one-dimensional time series $\chi(t) = \{x_t; t = 1, \ldots, M\}$, letting $n = D \geq 2$ be the number of immersion dimension ($D \in \mathbb{N}$) and τ be the delay time ($\tau \in \mathbb{N}$), to each time s, we assign a D-dimensional vector

$$(s) \rightarrow (x_{s-(D-1)\tau}, x_{s-(D-2)\tau}, \ldots, x_{s-(D-1)\tau}, x_s), \tag{A3}$$

which results from the evaluation of the time series χ at times $s - (D-1)\tau, s - (D-2), \ldots., s - \tau$ and s. It can be seen that the higher the value of D, the more temporal information is embedded in the patterns about the element's past.

Then, to the ordinal pattern of order D related to time s is associated the permutation $\pi = (r_0, r_1, \ldots, r_D - 1)$, that we simplify as $[0; 1; \cdots .; D-1]$, whose elements satisfy the relation

$$x_{s-r_{D-1}\tau} \leq x_{s-r_{D-2}\tau} \leq x_{s-r_1} \cdots \leq x_{s-r_0}. \tag{A4}$$

Thus, the vector defined in Eq. (A3) is represented by symbol π. Then, the total number of possible permutations π_i will be $D!$ when the immersion dimension is D.

As clarified above, $r_i < r_{i-1}$ is proposed if $x_{s-r_i\tau} = x_{s-r_{i-1}\tau}$ for unlikely cases where ambiguities exist.

The relative frequency can be simply computed according to the number of times that this particular order of sequence occurs in the time series divided by the total number of sequences,

$$p(\pi_i) = \frac{\#\{s | s \leq M - (D-1)\tau;\ (s) \text{ is of type } \pi_i\}}{M - (D-1)\tau}, \tag{A5}$$

where # denotes cardinality (number of occurrences). In this way, by applying the BPM to the time series χ, the PDF $P = \{p(\pi_i), i = 1, \ldots D!\}$ can be obtained by constructing the ordinal patterns.

Finally, for the generation of PDF by means of BPM, it is necessary to order the obtained probabilities in some way. In this work, we chose to use (among several existing options) the lexicographic ordering provided by Lehmer's algorithm due to the optimal distinction of different dynamics.[80,81] This algorithm consists of manipulation and generation of permutations in lexicographic order by using the factoradic system.

The following example is intended to clarify the methodology used. Let $\chi(t) = \{5, 6, 7, 14, 28, 10, 18\}$ be a time series with $M = 7$, and the BPM is applied in order to evaluate the PDF for $D = 3$ and $\tau = 1$. The vectors (5,6,7), (6,7,14), and (7,14,28) are represented by the ordinal pattern [012] as they are in strictly increasing order. On the other hand, (14,28,10) is represented by the pattern [120] and finally (28,10,18) is represented by [201]. In this case, from the permutation of immersion dimension, the number of possible states turns out to be $D! = 6$, which correspond to ordinal patterns seen in Fig. 16. The probabilities of occurrence associated with each mutually exclusive permutation are given by $p([012]) = 3/5$, $p([120]) = p([201]) = 1/5$, and $p([210]) = p([021]) = p([102]) = 0$. These results will end up generating the PDF $P = \{p_1, p_2, p_3, p_4, p_5, p_6\}$ associated with the time series χ. The last step in this process would be to apply Lehmer's algorithm to order them lexicographically.

c. General considerations for the calculation of quantifiers

The BPM can be applied to any type of time series, as long as a number of assumptions are satisfied. First of all, it is necessary that the time series possesses weak stationarity, i.e., that for $k \leq D$, the probability that $x_t < x_{t+k}$ must be independent of t,[42–44] which could be understood as "local" stationarity so that the calculated P tends to be exact. Another necessary condition is that the size of the time series is several orders of magnitude larger than the number of possible ordinal patterns, i.e., $M \gg D!$, in order to be able to work with reliable statistics and to be able to correctly differentiate deterministic dynamics from stochastic dynamics.[82] Besides conditioning the length of the time series, the immersion dimension D plays a very important role in the evaluation of appropriate probability distribution as it determines the number of accessible $D!$ states. Beyond the selected parameters, BP suggest working with $3 \leq D \leq 7$ and specifically consider a time delay of $\tau = 1$ (i.e., comparing immediate times).[42] However, other values of τ may provide additional information from the system,[75,80,81,83] where it has recently been shown that this parameter is intimately related, when relevant, to the intrinsic time scales of the system under analysis.[84,85]

Also, there are a couple of additional advantages of the application of BPM. The first is based on the simplicity that this technique can be employed, as it relies on the determination of only two parameters: the immersion dimension D and the delay time τ. The second advantage lies in the extremely fast computational processing of the algorithm.

In conclusion, the use of BPM to evaluate the PDF associated with the time series considers a series of partitions of relevant space of dimension D that reveals the relevant details of the ordinal structure of the given one-dimensional time series. This is equivalent to reconstructing a phase space with immersion dimension D and delay time τ. The symbolic representation of the time series by comparing consecutive ($\tau = 1$) or non consecutive ($\tau > 1$) allows

an accurate empirical reconstruction of the underlying phase space, even in the presence of weak noise (both observational and non-observational).[42] The BPM can be applied not only to time series corresponding to low-dimensional dynamical systems, but also to any type of time series (regular, chaotic, or noisy).

The application of BPM to time series of electrical records corresponding to local potentials has been extensively investigated.[86] In order to be able to characterize the dynamics of neuronal activity at mesoscopic scale (LFP), it is proposed to use permutation methodology for the evaluation of LFP associated to the time series and, thus, to calculate the information quantifiers.

The BPM provides a prescription for ordinary and global quantifiers of the entropic type (Shannon entropy and statistical complexity). Furthermore, having a PDF as $P = \{p_i; i = 1, \ldots, N\}$ makes $N!$ ways of ordering this data. This is why it is important to apply a sorting technique, such as the lexicographic ordering proposed by Lehmer, which was applied in this work to overcome the aforementioned problem.

In the present work, all information quantifiers were assessed using the BPM. When this methodology is used to calculate them, they are usually referred to as "permutation quantifiers," thus being "permutation entropy" and "MPR permutation complexity."

d. Calculation of the Shannon entropy and the statistical complexity

In order to characterize the dynamics of neuronal activity at a mesoscopic scale (LFP), the BPM was used to evaluate the time series associated with LFP in order to calculate information theory permutation quantifiers.

First, the causal information was estimated using BPM with embedding dimension $D = 3$, which satisfies the condition requested for having a reliable estimate if $M \gg D!$ (M length of the time series) is satisfied. Also, the delay time used was $\tau = 1$, which gives a convergent statistics and an optimal information quantifiers measure.[83] The estimations in the present work were performed for a time series of 10 min taking 4 s windows, which allowed us to have 2000 points for each window, ensuring $M = 2000 \gg D! = 6$ in all cases.

Moreover, BPM suggests the use of these setup of parameters, which are ideal for capturing the causal temporal characteristics of the signal under study in the current work. By this methodology, we estimated the PDF associated with each time series (for each channel of each electrode) from both types of LFP recordings (basal and preictal signals) and proceeded to construct the *PDF* corresponding to each of them. For having chosen $D = 3$, we had $D! = 3! = 6$ ordinal states. This methodology of analysis was repeated in data belonging to six subjects under study with refractory epilepsy.

Then, it was necessary to "organize" the ordinal pattern data obtained from the application of the BPM for correct construction of the PDF. As mentioned above, this was done by using Lehmer's algorithm. To apply this algorithm, we used a previously written computational code.[87]

The Shannon permutation entropy, H, and the permutation statistical complexity measure MPR, C, were calculated after finding the corresponding PDF for each channel for both preictal and basal signals from the Eqs. (A7) and (A8), respectively.

2. Shannon entropy

Information theory quantifiers correspond to measurements capable of characterizing a given property of the PDF associated to a time series linked to a physical observable, such as, for example, the electrical signal of the iEEG. The most paradigmatic example of this kind of information theory quantifier is the "Shannon entropy." Given a time series $\chi(t) \equiv \{x_i; t = 1, \ldots, M\}$ with M discrete values corresponding to the dynamics of a measured observable, the PF associated to it will be given by $P \equiv \{p_i; i = 1, \ldots N\}$, where $\sum_{i=1}^{N} p_i = 1$ and N are all the different i possible states of the system with associated probability of occurrence p_i. Then, the discrete Shannon entropy measure S[88] will be defined as

$$S[P] = -\sum_{i=1}^{N} p_i ln(p_i). \tag{A6}$$

It can be observed that this functional becomes null when it is possible to predict with complete certainty when the ith outcome will take place, that is, when $p_i = 1$ and $p_j = 0\ \forall j \neq i$. In such instance, the knowledge of the resulting process will be maximal. However, knowledge of the process will be minimal when the distribution is equiprobable, i.e., $p_i = 1/N\ \forall i$. Given these observations, it is possible to define the normalized Shannon entropy H as

$$H[P] = S[P]/S_{\max}, \tag{A7}$$

where $S_{\max} = ln(N)$ corresponds to the entropy of uniform distribution, resulting in $0 \leq H \leq 1$.

The normalized Shannon entropy H is a "global character" as information quantifier, since it is not sensitive to small perturbations in the values or to the rearrangement of PDF components.

a. Statistical complexity

Understanding the dynamics of epileptic seizures requires characterization of the complex structural dynamics of neuronal populations, their oscillatory organisation, and their role in the generation of such seizures. The human brain corresponds to a complex system on multiple time and space scales that has numerous subcomponents with a large number of interactions between them. This means that systems such as the human brain exhibit a non-trivial component-by-component relationship, and in order to understand its dynamics, it becomes necessary to quantify its complexity.

Complex systems are those that are highly composite and far from the "perfect order" (e.g., a regular crystal) and also to "complete disorder" (e.g., an ideal gas). From this outline, it is clear that the concept of complexity is linked to a possible hidden structure or patterns that characterize the dynamics that emerge from a system. For this reason, "statistical complexity" is considered as the information theory quantifier that indicates the "order" that systems possess.

In the various systems described, whether deterministic or of the random type, complexity will be characterized by the traces in their spatial and/or temporal correlation structures. It is important to note that the ordinal structures present in a process cannot be evaluated by just any quantifier. This means that a measure of statistical or structural complexity is necessary for a better characterization of the dynamics of the system represented by its time series.[89]

A complex system is built by a large number of mutually communicating elements with different kinds of interactions between its components, where each of these elements possesses different types of temporal patterns, and is further characterized by the dynamics that emerge from these different types of interactions. This is why the brain can be identified as a complex system in which the dynamical characteristics of the neuronal population emerge from the interactions of the neural network.

There exists a functional form for complexity, identified as C, which serves as a measure of the statistical complexity of a system and also meets the requirement mentioned above.[90] This measure quantifies the fine details of the dynamics of the system under investigation. In particular, the "statistical complexity" (MPR) can be expressed as[90]

$$C[P] = Q_J[P, P_e]H[P], \tag{A8}$$

where P is the PDF associated with the time series, P_e is the equiprobable distribution, $H[P]$ is the normalized Shannon entropy, and $Q_J[P, P_e]$ is the measure of non-equilibrium, which is a distance between P and P_e, and is given by

$$Q_J[P, P_e] = Q_0 J[P, P_e], \tag{A9}$$

where

$$J[P, P_e] = S\left[\frac{P + P_e}{2}\right] - \frac{S[P]}{2} - \frac{S[P_e]}{2} \tag{A10}$$

is the Jensen–Shannon divergence,[59,74] with S being the entropy given by Eq. (A6), and Q_0 a normalizing constant.

Since $J[P, P_e]$ reaches the maximum value when one of the components of P is equal to unity and the rest cancels, Q_0 of the Eq. (A9) is defined as the inverse of this maximum possible value, i.e.,

$$Q_0 = -2\left\{\frac{N+1}{N}\ln(N+1) - \ln(2N) + \ln N\right\}^{-1}, \tag{A11}$$

with N equal to the number of possible states of P. Thus, $0 \leq Q_J \leq 1$.

On the one hand, the use of Jensen–Shannon divergence has the utility of being able to compare symbolic compositions between different sequences,[91] since this divergence quantifies the difference between probability distributions. On the other hand, it is worth noting that the MPR complexity measure depends on only two different probability distributions, one associated with the system under analysis (P) and the other associated with the uniform distribution (P_e).

b. Causal information plane

Within statistical mechanics, it is interesting to be able to characterize isolated systems by means of their initial and arbitrary PDF. Also, the main goal of this area is to be able to describe the evolution of the system toward equilibrium, where without loss of generality it can be assumed that this state is given by uniform distribution $P_e = \{p_i = 1/N, \forall i = 1, \ldots, N\}$.

When evaluating information quantifiers and wishing to study their temporal dynamics, the temporal evolution can be analyzed using a two-dimensional diagram from the measurement of some quantifier as a function of time. On the other hand, the second law of thermodynamics states that for isolated systems, the entropy grows monotonically with time ($dH/dt \geq 0$).[92] This implies that the normalized Shannon entropy H can be considered as an arrow of time, and thus, it is possible to use this measure as a proxy for the time axis. Consequently, we can define the "causal information plane" for complexity as a function of entropy ($H \times C$).[59,93]

The concept of causality is given by the fact that temporal correlations between successive samples are taken into account when calculating the information quantifiers. This can be achieved through the BPM, which was used for the estimation of permutation entropy and complexity in this paper.

Indeed, the $H \times C$ plane is based only on global characteristics associated with the time series of the PDF. Since the complexity

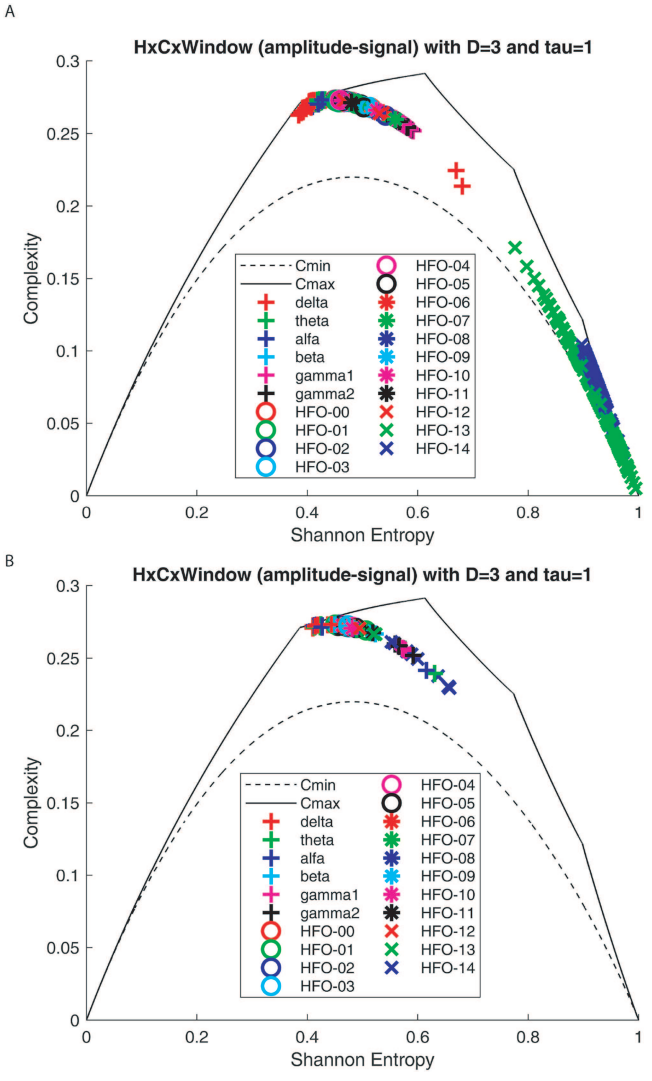

FIG. 17. $H \times C$-plane of the amplitude, fourth subject, taking into account different frequency bands. We consider $D = 3$ and $\tau = 1$. (a) Preictal state; (b) basal state.

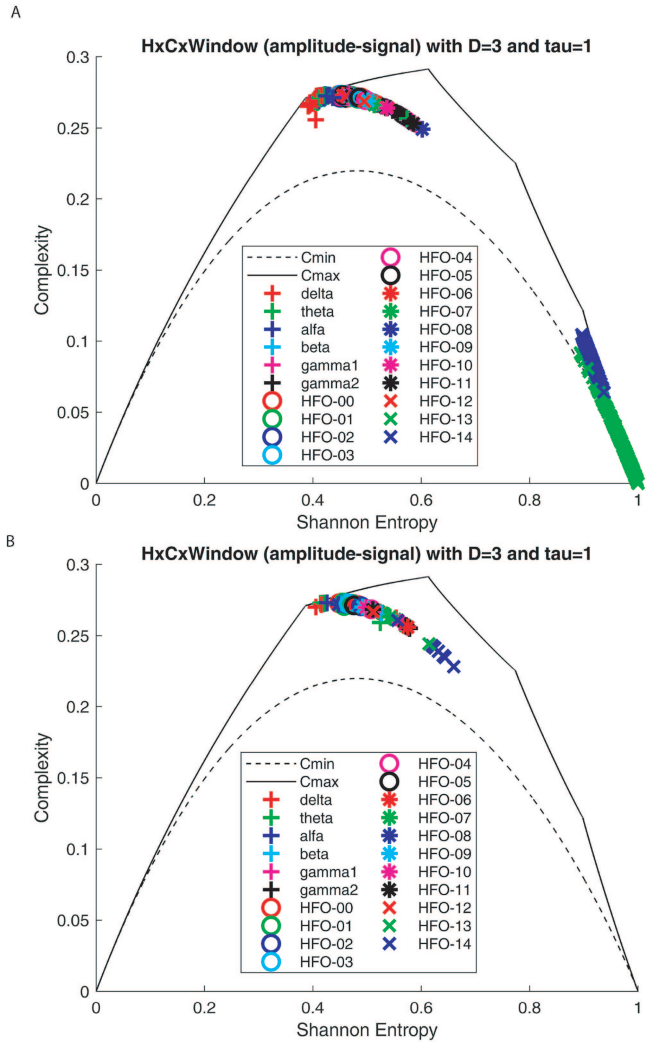

FIG. 18. $H \times C$-plane of the amplitude, fifth subject, taking into account different frequency bands. We consider $D = 3$ and $\tau = 1$. (a) Preictal state; (b) basal state.

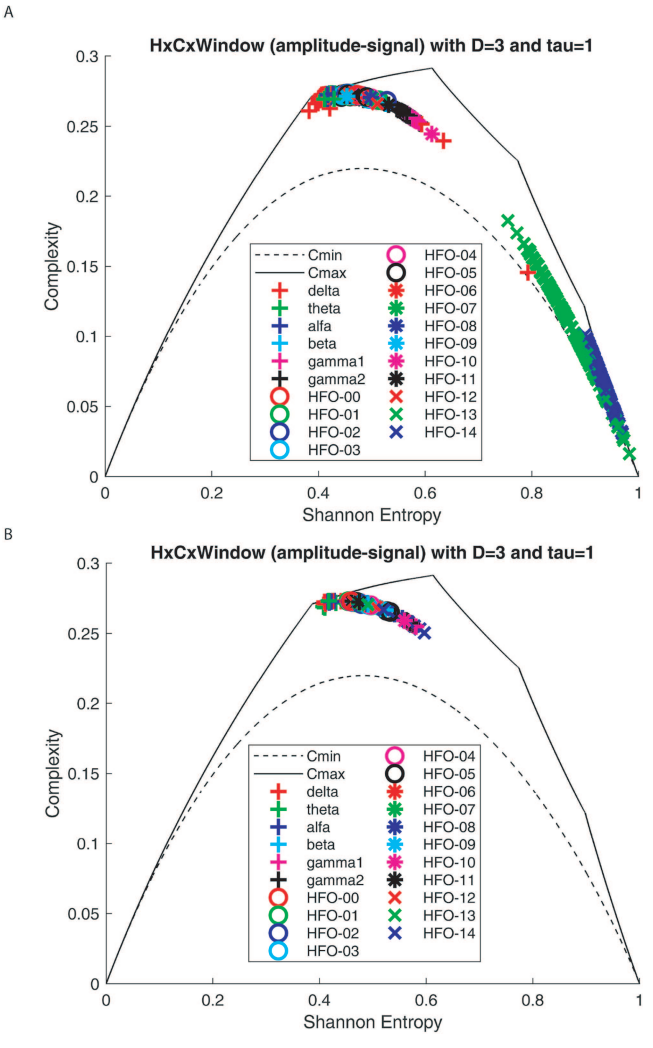

FIG. 19. $H \times C$-plane of the amplitude, sixth subject, taking into account different frequency bands. We consider $D = 3$ and $\tau = 1$. (a) Preictal state; (b) basal state.

is defined in terms of normalized Shannon entropy H [Eq. (A8)], it can be observed that for a given value of this magnitude, the range of possible values of C is determined between a $C_{\min}$ and a $C_{\max}$. This is due to the fact that the calculation of complexity depends on two different PDFs: one corresponding to the system under study P and the other being the uniform PDF P_e, thus restricting the possible values of the statistical complexity in the plane $H \times C$.[57] It can then be seen that evaluating C provides important additional information that the entropy measure did not provide, that is, related to the correlation structure between the components of the physical system.

c. $H \times C$ planes of the fourth, fifth, and sixth patients

The estimation of the $H \times C$ plane for the amplitude of the preictal signal is shown in Figs. 17(a), 18(a), and 19(a) for the fourth, fifth, and sixth patients, respectively, while, in contrast, the $H \times C$ plane of amplitude of the basal signals is depicted in Figs. 17(b), 18(b), and 19(b) for fourth, fifth, and sixth patients, respectively. The results for the $H \times C$ planes of the fourth, fifth, and sixth patients have a similar behavior to the one presented for first, second, and third subjects.

APPENDIX B: EXPERIMENTAL METHODS

The acquisition of experimental data from the iEEG registry of patients with refractory epilepsy was performed at the Hospital de Alta Complejidad "El Cruce," Florencio Varela, Argentina. The data acquisition was endorsed by the hospital's ethics committee, within

the framework of other work carried out on the patients. For consistency, we decided to use data obtained at the same research center and using the same data acquisition system. Data consistency may be critical as we consider that we are developing a novel principle with novel and important results for the investigation of preictal signal dynamics as an epileptogenic biomarker (with novel techniques combining signal phase and amplitude separation for different frequency bands of interest and investigating time series causality with BP). The purpose behind this decision is to always respect the same experimental protocol.

1. Data recording

The location and quantity of the electrodes are directly related to the variety and the number of cortical structures hypothesized as EZ. The task of intracranial electrode implantation is performed by the hospital's neurosurgeon, who does it by means of a stereotactic surgery. The location coordinates of each electrode are calculated using the Aimplan software (Micromar), a tool that allows the neurosurgeon to plan his stereotactic procedures with maximum precision. During stereotactic surgery, the neurosurgeon inserts the electrodes in the pre-planned location through the the stereotactic surgery. The correct implantation of the electrodes is then checked by imaging techniques, as can be seen in the Fig. 20.

The period of hospitalization will depend on the patient's predisposition to seizures during this period and usually lasts between 6 and 10 days. The signal obtained by the electrodes is amplified, bandpass filtered between 1 Hz and 2 KHz in order to acquire the HFO activity.

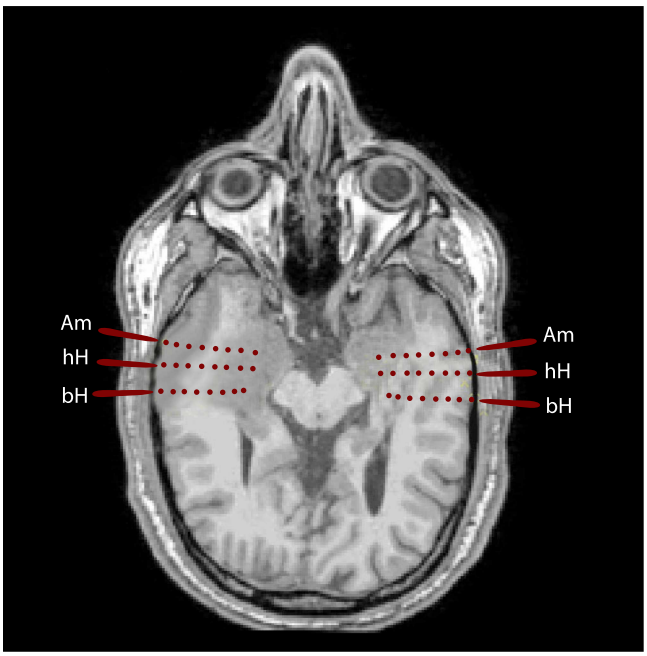

FIG. 20. Location of electrodes in reconstruction based on the fusion of computed axial tomography (CT scan) and magnetic resonance imaging (MRI) for one of the subjects. The electrodes are identified as follows: Am, amygdala; hH, hippocampal head; bH, hippocampal body (left side and right side).

The iEEG record is continuously and uninterruptedly stored in a computer intended for the acquisition of these data. These data are segmented by the measurement equipment approximately every 18 min (the exact time varies on the order of the hundredth of a second) and are stored in a specific format, which has metadata corresponding to the channel label, the sampling rate, the time of the sampling frequency, the start time of each recording, etc.

In order to analyze the dynamics that emerge in the moments prior to the epileptic seizure, it was decided to take the data from the record immediately prior to a seizure (preictal period) and another record far before the seizure (basal period). For the first one, the temporal onset of the epileptic seizure was identified from the clinical report drawn up by the neurologists team, which included the time of occurrence of the seizure. Then, the recording was split up discarding data after this time of onset. Thus, the data resulting from this segmentation have only preictal characteristics, from which a total sample of 10 min of duration was taken, prior to the onset of the event. For the "basal" record, a period of 10 min that occurred prior to the "preictal" record was taken as data, being this as close to the "preictal" record as possible. It should be noted that the temporal location of the basal recording occurs approximately 40 min before ictal onset. It is important to mention that this way of choosing the data to be analyzed is in agreement with the bibliographic findings regarding the duration of the preictal and basal periods.[52,53,94] On the other hand, the chosen seizure data had the condition that during the epileptic event at least some clinical manifestation was observed, i.e., it was not a subclinical seizure. Another important criterion was that the acquired signals should not be contaminated by high levels of artifacts in a large part of the recording. The recorded data were arranged in a matrix, where each column contained the time series acquired by each of the channels of the respective measurement electrodes and then processed in MATLAB.

The data used for the analysis of this work were the basal records (used as a control) and the preictal records of six patients under the hypotheses and specifications mentioned in Appendix A. The iEEG measured signal consists basically of the recording activity from eight active channels (plus a common reference channel) for each implanted intracranial electrode with a sampling rate of 2 kHz. We report results from 16 experimental sessions in six patients with drug-resistant epilepsy who were candidates for surgery (all right-handed, six males, 19–49 years old). Patients were implanted with chronic depth electrodes at "Hospital El Cruce" in Buenos Aires, Argentina. They were monitored 24/7, for seven to ten days, to determine the epileptogenic region for possible surgical resection.[95,96] A written informed consent was signed by each patient to participate in this study. All the experimental procedures were carried out in accordance to the Declaration of Helsinki and approved by "Hospital El Cruce" Medical Institutional Review Board. In particular, the first patient had implanted five electrodes (40 channels), and the second to sixth patient had six electrodes (48 channels). Each electrode probe had a total of nine microwires at its end, eight active recording channels and one (low impedance) reference (AD-TECH Medical Instrument Corporation, Wisconsin, USA). Electrode locations in hippocampus (11 probes) and amygdala (eight probes) were based exclusively on clinical criteria

TABLE I. Frequency bands analyzed. From 90 to 240 Hz, the spectrum was subdivided into consecutive 10 Hz bands, each band being named "HFO" together with the index associated with its ordinal.

Band	F (Hz)	Band	F (Hz)
Delta	[0.5, 4)	HFO 5	(140, 150]
Theta	[4, 8)	HFO 6	(150, 160]
Alpha	[8, 12)	HFO 7	(160, 170]
Beta	[12, 30)	HFO 8	(170, 180]
Gamma1	[30, 60)	HFO 9	(180, 190]
Gamma2	[60, 90)	HFO 10	(190, 200]
HFO 0	[90, 100)	HFO 11	(200, 210]
HFO 1	[100, 110]	HFO 12	(210, 220]
HFO 2	(110, 120]	HFO 13	(220, 230]
HFO 3	(120, 130]	HFO 14	(230, 240]
HFO 4	(130, 140]	...	...

and were verified by CT co-registered to preoperative MRI. The signals were recorded using a 128-channel Cervello Elite EEG System (Blackrock Microsystems, UT, USA), with a sampling rate of 2 kHZ.

2. Frequency band filtering

To increase the resolution of the signal and to remove interference such as $1/f$ noise, we filtered the signal between 0.5 and 240 Hz using filtering based on "Kaiser windows,"developed by Belitski.[56] The parameters of this filtering consisted of a sharp transition bandwidth of 0.1 Hz, a small passband ripple of 0.05 dB, and a high band-clearing attenuation of 60 dB. We selected this filter particularly for its versatility, as it is widely used in a vast number of studies for that reason. It is important to point out that when applied, we observed how the signal is "smoothed" at its extremes.

In addition to Kaiser filtering, a bandpass filter was also performed, where the filtered bands can be seen in Table I.

The first frequency bands (from 1–90 Hz) correspond to the traditional Berger's[97] oscillation bands, while the higher bands correspond to HFO ripples, where each of them was subdivided into consecutive intervals of 10 Hz. Fourier transform was applied to the filtered signal to visualize and corroborate the correct filtering of each frequency band for both basal and preictal recordings.

REFERENCES

[1] G. Buzsaki, *Rhythms of the Brain* (Oxford University Press, 2006).
[2] E. M. Izhikevich, Neural Comput. **18**, 245 (2006).
[3] G. Buzsáki and A. Draguhn, Science **304**, 1926 (2004).
[4] M. R. Deans, J. R. Gibson, C. Sellitto, B. W. Connors, and D. L. Paul, Neuron **31**, 477 (2001).
[5] M. DeWeese and A. Zador, J. Neurosci. **26**, 12206 (2006).
[6] V. Bhandawat, S. Olsen, N. Gouwens, and S. M. L. R. Wilson, Nat. Neurosci. **10**, 1474 (2007).
[7] M. A. Montemurro, M. J. Rasch, Y. Murayama, N. K. Logothetis, and S. Panzeri, Curr. Biol. **18**, 375 (2008).
[8] K. Mizuseki and G. Buzsáki, Cell Rep. **4**, 1010 (2013).
[9] G. Buzsáki and K. Mizuseki, Nat. Rev. Neurosci. **15**, 264 (2014).
[10] G. Buzsáki, Science **347**, 612 (2015).
[11] L. Montangie and F. Montani, Physica A **471**, 845 (2017).
[12] R. Baravalle and F. Montani, Phys. Rev. E **103**, 042308 (2021).
[13] R. Baravalle, O. Rosso, and F. Montani, Chaos **28**, 075513 (2018).
[14] R. Baravalle, O. Rosso, and F. Montani, Physica A **511**, 27 (2018).
[15] R. Baravalle, N. Guisande, M. Granado, O. A. Rosso, and F. Montani, Front. Phys. **7**, 115 (2019).
[16] X. Wang, Physiol. Rev. **90**, 1195 (2010).
[17] C. Hammond, H. Bergman, and P. Brown, Trends Neurosci. **30**, 357 (2007).
[18] G. Deco and A. Thiele, Eur. J. Neurosci. **30**, 347 (2009).
[19] G. Thut, C. Miniussi, and J. Gross, Curr. Biol. **22**, 658 (2012).
[20] P. Allen, D. Fish, and S. Smith, Electroencephalogr. Clin. Neurophysiol. **82**, 155 (1992).
[21] A. Bragin, J. Engel, Jr., C. L. Wilson, I. Fried, and G. Buzsáki, Hippocampus **9**, 137 (1999).
[22] J. Jefferys, Physiol. Rev. **75**, 689 (1995).
[23] R. D. Traub, A. Draguhn, M. A. Whittington, T. Baldeweg, A. Bibbig, E. H. Buhl, and D. Schmitz, Rev. Neurosci. **13**, 1 (2002).
[24] V. I. Dzhala and K. J. Staley, J. Neurosci. **24**, 8896 (2004).
[25] P. Jiruska, C. Alvarado-Rojas, C. A. Schevon, R. Staba, W. Stacey, F. Wendling, and M. Avoli, Epilepsia **58**, 1330 (2017).
[26] J. Jirsch, E. Urrestarazu, P. LeVan, A. Olivier, F. Dubeau, and J. Gotman, Brain **129**, 1593 (2006).
[27] H. Khosravani, N. Mehrotra, M. Rigby, W. J. Hader, C. R. Pinnegar, N. Pillay, S. Wiebe, and P. Federico, Epilepsia **50**, 605 (2009).
[28] R. Zelmann, M. Zijlmans, J. Jacobs, C.-E. Châtillon, and J. Gotman, Clin. Neurophysiol. **120**, 1457 (2009).
[29] M. A. van't Klooster, N. E. van Klink, W. J. Zweiphenning, F. S. Leijten, R. Zelmann, C. H. Ferrier, P. C. van Rijen, W. M. Otte, K. P. Braun, G. J. Huiskamp *et al.*, Ann. Neurol. **81**, 664 (2017).
[30] J. Jacobs, M. Zijlmans, R. Zelmann, C.-É. Chatillon, J. Hall, A. Olivier, F. Dubeau, and J. Gotman, Ann. Neurol. **67**, 209 (2010).
[31] P. Ryvlin, J. H. Cross, and S. Rheims, Lancet Neurol. **13**, 1114 (2014).
[32] J. Wu, R. Sankar, J. Lerner, J. Matsumoto, H. Vinters, and G. Mathern, Neurology **75**, 1686 (2010).
[33] H. Fujiwara, H. M. Greiner, K. H. Lee, K. D. Holland-Bouley, J. H. Seo, T. Arthur, F. T. Mangano, J. L. Leach, and D. F. Rose, Epilepsia **53**, 1607 (2012).
[34] J. Jacobs, P. LeVan, R. Chander, J. Hall, F. Dubeau, and J. Gotman, Epilepsia **49**, 1893 (2008).
[35] M. Zijlmans, P. Jiruska, R. Zelmann, F. S. Leijten, J. G. Jefferys, and J. Gotman, Ann. Neurol. **71**, 169 (2012).
[36] M. Granado, R. Baravalle, and F. Montani, Anales (Asociación Física Argentina) **31**, 67 (2020).
[37] M. Zijlmans, J. Jacobs, R. Zelmann, F. Dubeau, and J. Gotman, Epilepsy Res. **85**, 287 (2009).
[38] A. Bragin, C. L. Wilson, and J. Engel, Jr., Epilepsia **48**, 35 (2007).
[39] O. Rosso and C. Masoller, Phys. Rev. E **79**, 040106(R) (2009).
[40] O. Rosso and C. Masoller, Eur. Phys. J. B **69**, 37 (2009).
[41] F. Montani and O. Rosso, Entropy **16**, 4677 (2014).
[42] C. Bandt and B. Pompe, Phys. Rev. Lett. **88**, 174102 (2002).
[43] I. Leyva, J. H. Martínez, C. Masoller, O. A. Rosso, and M. Zanin, Europhys. Lett. **138**, 31001 (2022).
[44] H. Kang, X. Zhang, and G. Zhang, Physica A **568**, 125686 (2021).
[45] A. Krumholz, Ann. Neurol. **45**, 825 (1999).
[46] N. I. for Health and C. Excellence: National Clinical Guideline Centre (UK) (2012).
[47] S. J. McPhee, G. D. Hammer, and M.-H. Education, *Pathophysiology of Disease: An Introduction to Clinical Medicine* (McGraw-Hill Medical, New York, 2010).
[48] P. Rutecki, *Ions in the Brain: Normal Function, Seizures, and Stroke* (Oxford University Press, New York, 2004), p. 16.
[49] P. Jiruska, P. M. de Curtis, J. G. Jefferys, C. A. Schevon, S. J. Schiff, and K. Schindler, "Synchronization and desynchronization in epilepsy: controversies and hypotheses," J Physiol. **591**(4), 787–797 (2013).
[50] See https://www.epilepsy.com/what-is-epilepsy/seizure-types#How-are-different-symptoms-during-a-seizure-described? for "Epilepsy Foundation of Colorado, USA epilepsy brochure" (2022).
[51] H. H. Lange, J. P. Lieb, J. Engel, and P. H. Crandall, Electroencephalogr. Clin. Neurophysiol. **56**, 543 (1983).

[52]M. E. Weinand, L. P. Carter, W. F. El-Saadany, P. J. Sioutos, D. M. Labiner, and K. J. Oommen, J. Neurosurg. **86**, 226 (1997).
[53]C. Baumgartner, W. Serles, F. Leutmezer, E. Pataraia, S. Aull, T. Czech, U. Pietrzyk, A. Relic, and I. Podreka, J. Nucl. Med. **39**(6), 978–982 (1998).
[54]B. Litt and J. Echauz, Lancet Neurol. **1**, 22 (2002).
[55]M. Le Van Quyen, J. Foucher, J.-P. Lachaux, E. Rodriguez, A. Lutz, J. Martinerie, and F. J. Varela, J. Neurosci. Methods **111**, 83 (2001).
[56]A. Belitski, A. Gretton, C. Magri, Y. Murayama, M. A. Montemurro, N. K. Logothetis, and S. Panzeri, J. Neurosci. **28**, 5696 (2008).
[57]M. Martin, A. Plastino, and O. Rosso, Physica A **369**, 439 (2006).
[58]O. A. Rosso, F. Olivares, L. Zunino, L. De Micco, A. L. Aquino, A. Plastino, and H. A. Larrondo, Eur. Phys. J. B **86**, 116 (2013).
[59]O. Rosso, H. Larrondo, M. Martin, A. Plastino, and M. Fuentes, Phys. Rev. Lett. **99**, 154102 (2007).
[60]O. A. Rosso, L. C. Carpi, P. M. Saco, M. G. Ravetti, A. Plastino, and H. A. Larrondo, Physica A **391**, 42 (2012).
[61]O. A. Rosso, L. C. Carpi, P. M. Saco, M. G. Ravetti, H. A. Larrondo, and A. Plastino, Eur. Phys. J. B **85**, 419 (2012).
[62]O. Rosso and C. Masoller, Eur. Phys. J. B **69**, 37 (2009).
[63]S. T. Herman, Neurology **59**, S21 (2002).
[64]E. M. Goldberg and D. A. Coulter, Nat. Rev. Neurosci. **14**, 337 (2013).
[65]H. Luders, in *Surgical Treatment of the Epilepsies*, 2nd ed., edited by J. Engel, Jr. (Raven Press, NY, 1993), pp. 137–153.
[66]S. S. Spencer, Epilepsia **43**, 219 (2002).
[67]A. Blenkmann, G. Seifer, J. P. Princich, D. Consalvo, S. Kochen, and C. Muravchik, Epilepsy Res. **98**, 223 (2012).
[68]P. Malerba, G. P. Krishnan, J.-M. Fellous, and M. Bazhenov, PLoS Comput. Biol. **12**, e1004880 (2016).
[69]G. Curio, B.-M. Mackert, M. Burghoff, R. Koetitz, K. Abraham-Fuchs, and W. Härer, Electroencephalogr. Clin. Neurophysiol. **91**, 483 (1994).
[70]B. Crépon, V. Navarro, D. Hasboun, S. Clemenceau, J. Martinerie, M. Baulac, C. Adam, and M. Le Van Quyen, Brain **133**, 33 (2009).
[71]C. Heumann and M. Schomaker Shalabh, *Introduction to Statistics and Data Analysis* (Springer, Switzerland, 2016).
[72]H. Fourati and D. E. C. Belkhiat, *Multisensor Attitude Estimation: Fundamental Concepts and Applications* (CRC Press, 2016).
[73]J. K. Ord, *Families of Frequency Distributions* (Griffin, 1972).
[74]O. A. Rosso and C. Masoller, Phys. Rev. E **79**, 040106 (2009).
[75]O. A. Rosso, F. Olivares, and A. Plastino, Papers Phys. **7**, 070006 (2015).
[76]M. P. Dafilis, F. Frascoli, P. J. Cadusch, and D. T. Liley, Physica D **238**, 1056 (2009).
[77]D. H. Wolpert and D. R. Wolf, Phys. Rev. E **52**, 6841 (1995).
[78]P. M. Saco, L. C. Carpi, A. Figliola, E. Serrano, and O. A. Rosso, Physica A **389**, 5022 (2010).
[79]S. Berger, G. Schneider, E. Kochs, and D. Jordan, Entropy **19**, 692 (2017).
[80]F. Olivares, A. Plastino, and O. A. Rosso, Physica A **391**, 2518 (2012).
[81]F. Olivares, A. Plastino, and O. A. Rosso, Phys. Lett. A **376**, 1577 (2012).
[82]A. Kowalski, M. Martín, A. Plastino, and O. Rosso, Physica D **233**, 21 (2007).
[83]L. Zunino, M. C. Soriano, I. Fischer, O. A. Rosso, and C. R. Mirasso, Phys. Rev. E **82**, 046212 (2010).
[84]M. C. Soriano, L. Zunino, O. A. Rosso, I. Fischer, and C. R. Mirasso, IEEE J. Quantum Electron. **47**, 252 (2011).
[85]L. Zunino, M. C. Soriano, and O. A. Rosso, Phys. Rev. E **86**, 046210 (2012).
[86]M. Zanin, L. Zunino, O. A. Rosso, and D. Papo, Entropy **14**, 1553 (2012).
[87]K. Schwarz, See https://bit.ly/2HorA88 for "Factoradic Permutation algorithm" (2013).
[88]C. Shannon and W. Weaver, *The Mathematical Theory of Communication* (University of Illinois Press, Champaign, IL, 1949).
[89]D. P. Feldman and J. P. Crutchfield, Phys. Lett. A **238**, 244 (1998).
[90]M. Martin, A. Plastino, and O. Rosso, Phys. Lett. A **311**, 126 (2003).
[91]I. Grosse, P. Bernaola-Galván, P. Carpena, R. Román-Roldán, J. Oliver, and H. E. Stanley, Phys. Rev. E **65**, 041905 (2002).
[92]A. R. Plastino and A. Plastino, Phys. Rev. E **54**, 4423 (1996).
[93]F. Montani, E. B. Deleglise, and O. A. Rosso, Physica A **401**, 58 (2014).
[94]P. Rajna, B. Clemens, E. Csibri, E. Dobos, A. Geregely, M. Gottschal, I. György, Á. Horváth, F. Horváth, L. Mezöfi, I. Velkey, J. Veres, and E. Wagner, Seizure **6**, 361 (1997).
[95]H. Rey, M. Ison, C. Pedreira, A. Valentin, G. Alarcon, R. Selway, M. Richardson, and R. Quian Quiroga, J. Anat. **227**, 394 (2015).
[96]H. Rey, B. Gori, F. Chaure, S. Collavini, A. Blenkmann, P. Seoane, E. Seoane, S. Kochen, and R. Quian Quiroga, Curr. Biol. **30**, 1152 (2020).
[97]G. Schalk and J. Mellinger, *A Practical Guide to Brain–Computer Interfacing with BCI2000: General-Purpose Software for Brain-Computer Interface Research, Data Acquisition, Stimulus Presentation, and Brain Monitoring* (Springer Science & Business Media, 2010).